Effects of AGN feedback on ΛCDM galaxies

Claudia del P. Lagos,[1][*] Sofía A. Cora[2,3] and Nelson D. Padilla[1]

[1]*Departamento Astronomía y Astrofísica, Pontificia Universidad Católica de Chile, Av. Vicuña Mackenna 4860, Stgo., Chile*
[2]*Facultad de Ciencias Astronómicas y Geofísicas de la Universidad Nacional de La Plata, and Instituto de Astrofísica de La Plata (CCT La Plata, CONICET, UNLP), Observatorio Astronómico, Paseo del Bosque S/N, 1900 La Plata, Argentina*
[3]*Consejo Nacional de Investigaciones Científicas y Técnicas, Rivadavia 1917, Buenos Aires, Argentina*

ABSTRACT

We study the effects of active galactic nuclei (AGN) feedback on the formation and evolution of galaxies by using a combination of a cosmological *N*-body simulation of the concordance Lambda cold dark matter (ΛCDM) paradigm and a semi-analytic model of galaxy formation. This model is an improved version of the one described by Cora (2006), which now considers the growth of black holes (BHs) as driven by (i) gas accretion during merger-driven starbursts and mergers with other BHs, (ii) accretion during starbursts triggered by disc instabilities and (iii) accretion of gas cooled from quasi-hydrostatic hot gas haloes. It is assumed that feedback from AGN operates in the last case. The model has been calibrated in order to reproduce observational correlations between BH mass and mass, velocity dispersion and absolute magnitudes of the galaxy bulge. AGN feedback has a strong impact on reducing or even suppressing gas cooling, an effect that becomes important at lower redshifts. This phenomenon helps to reproduce the observed galaxy luminosity function (LF) in the optical and near-infrared bands at $z = 0$, and the cosmic star formation rate and stellar mass functions over a wide redshift range ($0 \lesssim z \lesssim 5$). It also allows us to have a population of massive galaxies already in place at $z \gtrsim 1$, which are mostly early-type and have older and redder stellar populations than lower mass galaxies, reproducing the observed bimodality in the galaxy colour distribution, and the morphological fractions. The evolution of the optical QSO LF is also reproduced, provided that the presence of a significant fraction of obscured QSOs is assumed. We explore the effects of AGN feedback during starbursts finding that, in order to obtain a good agreement with observations, these need to be strong enough to expel the reheated gas away from the galaxy halo. We also test new, recent prescriptions for dynamical friction time-scales, and find that they produce an earlier formation of elliptical galaxies, and a larger amount of disc instabilities, which compensate the change in the merger frequency such that the properties of $z = 0$ galaxies remain almost unaffected.

Key words: galaxies: evolution – galaxies: formation – quasars: general – galaxies: statistics.

1 INTRODUCTION

Over the last decade, there has been a phenomenal increase in the range and quantity of data on quasi-stellar objects (QSOs) or 'quasars' and galaxies with active galactic nuclei (AGN), which are the seats of an intense production of energy. They were singled out from the general galaxy population by their peculiar colours, morphology and/or strong emission in the radio, X-ray or infrared bands. The conventional view regards QSOs and AGN as different manifestations of the same phenomenon. Observations of the brightest Seyfert galaxies, one of the types in which AGN are classified, show

events of sudden bursts of star formation activity (starbursts) that occurred 1–2 Gyr ago; these events have been associated, by some authors, with galaxy mergers (Sanders & Mirabel 1996; Kauffmann 2003). Recent results by Feain et al. (2007) show direct evidence of the QSO–star formation connection where 70 per cent of the quasar radio emission comes from star formation activity of the host galaxy.

In a pioneering work by Hoyle & Fowler (1963), it was proposed that the energy from AGN was of gravitational origin derived from the collapse of very massive objects under their own strong gravitational fields. These early ideas found a modified expression in the paradigm of black hole (BH) accretion discs a few years later (Lynden-Bell 1969). In more recent times, an important connection between AGN and galaxy evolution has been deduced from

[*]E-mail: clagos@astro.puc.cl

the correlation between BHs, thought to be the engines of AGN, and properties of the host galaxy such as the bulge mass (Häring & Rix 2004), the luminosity in the *K*, *B* and *V* bands, the stellar mass (Marconi & Hunt 2003), and the velocity dispersion of the stars in the bulge (Ferrarese & Merrit 2000). The existence of a galactic bulge has been thought to be related to merger events, which led to speculate that mergers may drive the formation and evolution of BHs. Furthermore, Boyle & Terlevich (1998) show a correlation between the evolution of the global stellar formation rate and the luminosity density of optically selected quasars. This could also indicate that BHs are related to merger events and, therefore, to starburst phenomena as many authors have speculated (e.g. Bower et al. 2006; Croton et al. 2006; Malbon et al. 2007; Sijacki et al. 2007).

The alleged link between AGN and star formation activity brings questions related to the effect of this nuclear activity on the evolution of their host galaxies or galaxy clusters. Many recent observational results have begun to answer some of these questions complementing our picture of galaxy formation and evolution. For example, Schawinski et al. (2007) find a population of early-type galaxies lying outside the red sequence in the colour–magnitude diagram; this red population comprises star-forming and Seyfert galaxies. From these data, they identify an evolutionary sequence from star-forming (blue population) to quiescent galaxies (red population). This transition is explained by the effect of an AGN phase occurring roughly 0.5 Gyr after the starburst, which suppresses star formation. Reuland et al. (2007) have been able to confirm this result at high redshifts.

Direct observational evidence of AGN activity is provided by radio galaxies and quasars containing jets that transport energy from the AGN to the surrounding medium. The effects of jets issuing from AGN have been observed in many different wavelengths. Radio sources show large-scale outflows of significant gas masses which are generated by radio jets (Nesvadba et al. 2006, 2007; Temi, Brighenti & Mathews 2007). Theoretical studies of jets indicate that the time-scales for transient activity (e.g. restoration of equilibrium, buoyant transport in the hot gas) are consistent with a release of feedback energy from a central BH (Temi et al. 2007). The dichotomy in the properties of low- and high-excitation radio galaxies has been interpreted as an additional contribution from cold gas acting in high-excitation sources that forms the cold disc and torus around a central engine (Evans, Hardcastle & Croston 2007). Observations in X-rays indicate the presence of shocks, bubbles and sound waves thought to be driven by nuclear activity and to be responsible for heating the cluster core, as in the Perseus cluster (Sanders 2007, and references therein).

All these results illustrate the key role of AGN on galaxy evolution. As AGN have become a crucial ingredient of the galaxy evolution process, many theoretical works have proposed different possible scenarios for BH growth and the associated AGN feedback. These works include pure analytic approximations (e.g. Efstathiou & Rees 1988; Percival & Miller 1999; Churazov et al. 2002; Hopkins et al. 2007), semi-analytic models of galaxy formation (e.g. Kauffmann & Haehnelt 2000; Cattaneo 2001; Enoki, Nagashima & Gouda 2003; Granato et al. 2004; Cattaneo et al. 2005; Bower et al. 2006; Cattaneo et al. 2006; Croton et al. 2006; Menci et al. 2006; Malbon et al. 2007; Marulli et al. 2008), and fully self-consistent numerical models (Springel et al. 2005a; Sijacki et al. 2007). The application of a semi-analytic model of galaxy formation on a cosmological numerical simulation has demonstrated to be a very appropriate tool for the study of phenomena that drive the formation and evolution of galaxies within the hierarchical clustering scenario. This is the method used to investigate the effects of AGN feedback in the present work.

Our semi-analytic model is based on the one described by Cora (2006), to which we refer to as SAG1 (acronym for 'semi-analytic galaxies' version 1). This model follows the formation and evolution of galaxies including gas cooling, star formation, SNe explosions and mergers, as well as a detailed implementation of metal enrichment of stars and interstellar and intergalactic medium. SAG1, as well as many other semi-analytic models, reproduce to a reasonable degree observational results such as gas fractions, luminosity functions (LF), the Tully–Fisher (TF) relation, and galaxy colours. However, some inconsistencies still persist, in particular, the existence of a blue massive galaxy population and an excess of bright galaxies in the LF compared with observations in the b_J and K band (e.g. Cole et al. 2000; Springel et al. 2001; Baugh et al. 2004). These problems are in part due to the fact that the mass function of host dark matter haloes does not show a sharp cut-off at masses corresponding to L^* galaxies in the model. Therefore, models that populate these haloes tend to produce too many bright galaxies (Baugh 2006). The implementation of an artificial suppression of gas cooling made in SAG1, that affects haloes characterized by a virial velocity higher than a certain threshold, was a simple solution to overcome, at least partially, the inconsistencies mentioned above. These problems call for the inclusion of additional processes in order to reconcile, to a further degree, model results with observations. The physical process thought to be responsible for the control of the amount of gas that can cool is AGN feedback, which is triggered by gas accretion events on to central supermassive BHs. Recent works have made progress in this sense, demonstrating that AGN feedback is crucial to reduce gas cooling in large haloes, thus preventing them from forming stars at late times and being able to explain the exponential cut-off in the bright end of the galaxy LF (e.g. Bower et al. 2006; Cattaneo et al. 2006; Croton et al. 2006; Menci et al. 2006; Malbon et al. 2007). Following the prescriptions implemented in these works, we replace the simple procedure of stopping gas cooling in haloes with high virial velocity, as it is implemented in SAG1, by a more physical modelling of AGN feedback in galaxies, giving raise to the version SAG2.

The currently implemented models of AGN feedback only prevents significant gas cooling in large haloes. The so called *radio mode* feedback (see for instance, Croton et al. 2006) is assumed to produce low energy 'radio' activity. Recent observational results by Gastadello et al. (2007) on the galaxy cluster AWM 4 cannot be explained if AGN activity only produces this mode of feedback, since it presents an active radio source which is not accompanied by an X-ray temperature gradient; this might indicate the presence of AGN feedback during high accretion rates originated during mergers and disc instabilities, which also feed the BH growth. We explore this possibility within the Lambda cold dark matter (ΛCDM) framework using SAG2.

Our model SAG2 is also used to investigate the impact of new theoretical merger time-scales presented in two parallel studies carried out by Jiang et al. (2007) and Boylan-Kolchin, Ma & Quataert (2007). These works show that the equation for merger time-scales given by Lacey & Cole (1993) systematically underestimates the time-scales of minor mergers and overestimates those of major mergers.

This work is organized as follows. Section 2 presents a description of the cosmological simulation used and the improved semi-analytic model SAG2, summarizing first the original model SAG1 and then giving a detailed description of the AGN feedback model introduced. Section 3 describes the behaviour of BH and QSO properties in the

model, and presents the analysis of the effects of AGN feedback on galaxy properties. Further improvements made to SAG2, including the effects of starburst AGN feedback, and new prescriptions for merger time-scales, are presented in Section 4. Finally, Section 5 gives the main conclusions of this work.

2 A HYBRID MODEL OF GALAXY FORMATION AND EVOLUTION

We study the formation and evolution of galaxies by applying a numerical technique which combines a cosmological N-body simulation of the concordance ΛCDM universe and a semi-analytic model of galaxy formation. In this hybrid model, the outputs of the cosmological simulation are used to construct merger histories of dark matter haloes which are used by the semi-analytic code to generate the galaxy population. The main advantage of semi-analytic codes is that they allow us to reach a larger dynamic range than fully self-consistent simulations, at a far smaller computational cost.

The semi-analytic model used here is based on that described by Cora (2006) (SAG1)). The physical processes considered in this model are cooling of hot gas as a result of radiative losses, star formation, feedback from supernova (SN) explosions and galaxy mergers, modelled as in Springel et al. (2001). The model also tracks the circulation of metals between the different baryonic components, that is, cold gas, hot diffuse gas and stars, following the model described by De Lucia, Kauffmann & White (2004), with the additional advantage of including the mass evolution of different chemical elements.

In the present work, SAG1 is improved by including feedback from AGN as a replacement of the artificial suppression of gas cooling in massive haloes, thus leading to the version SAG2. In the following subsections, we present the main characteristics of the N-body simulation used, and briefly describe the physical processes already included in SAG1. In the original version of the code, only major mergers trigger starbursts; we now include two other mechanisms responsible of this kind of events, minor mergers and disc instabilities. Then, we present the model of BH growth and the associated AGN feedback implemented in the new version of the code.

2.1 ΛCDM cosmological simulation

We use a cosmological simulation of the concordance ΛCDM cosmology in a periodic box of $60\,h^{-1}$ Mpc. This box is large enough to allow us to make a suitable analysis of the LF of galaxies and quasars, and of the galaxy mass function. The simulation contains $16\,777\,216$ dark matter particles with a mass resolution of $1.001 \times 10^9\,h^{-1}\,\mathrm{M_{\odot}}$. More than $54\,000$ dark matter haloes have been identified, with the largest one having a mass of $5.36 \times 10^{14}\,h^{-1}\,\mathrm{M_{\odot}}$.

The simulation parameters are consistent with the results of *Wilkinson Microwave Anisotropy Probe* data (Spergel 2003), that is, $\Omega_{\mathrm{m}} = \Omega_{\mathrm{DM}} + \Omega_{\mathrm{baryons}} = 0.28$ (with a baryon fraction of 0.16), $\Omega_{\Lambda} = 0.72$ and $\sigma_8 = 0.9$. The Hubble constant is $H_0 = 100\,h\,\mathrm{Mpc^{-1}}$, with $h = 0.72$. The gravitational softening length, ϵ, is $3.0\,h^{-1}$ kpc. The simulation starts from a redshift $z = 48$ and is run using the public version of the GADGET-2 code (Springel 2005b).

Dark haloes are first identified as virialized particle groups by a friends-of-friends (FOF) algorithm. A SUBFIND algorithm (Springel et al. 2001) is then applied to these groups in order to find self-bound dark matter substructures. Merger trees are then constructed from these dark matter haloes and their embedded substructures.

2.2 Semi-analytic model SAG1

We briefly comment the processes of gas cooling, star formation, SN feedback and metal production included in the model SAG1; we refer the reader to Cora (2006) for a more detailed description.

We assume that hot gas always fills the dark matter haloes following an isothermal distribution. Initially, the hot gas mass is given by the baryon fraction of the virial mass of the dark matter halo. It is subsequently modified by the amount of gas that has cooled and the stellar mass formed in the galaxies contained within the halo. The mass of hot gas that cools in each dark matter halo in the underlying cosmological simulation is given by the cooling rate

$$\frac{\mathrm{d}M_{\mathrm{cool}}}{\mathrm{d}t} = 4\pi\rho_{\mathrm{g}}r_{\mathrm{cool}}^2\frac{\mathrm{d}r_{\mathrm{cool}}}{\mathrm{d}t}, \tag{1}$$

where ρ_{g} is the density profile of an isothermal sphere, and r_{cool} is the cooling radius. The local cooling time is defined as the ratio between the specific thermal energy content of the gas and the cooling rate per unit volume, $\Lambda(T, Z)$, which depends of the metallicity (Sutherland & Dopita 1993), and the temperature $T = 35.9(V_{\mathrm{vir}}/\mathrm{km\,s^{-1}})$ of the halo, being V_{vir} its virial velocity. This process only operates when the galaxy is the central galaxy of a given halo. The cooled gas contributes to the formation of the galaxy disc. The cold gas mass of each galaxy is involved in the star formation process. The star formation rate is given by

$$\frac{\mathrm{d}M_{\star}}{\mathrm{d}t} = \frac{\alpha M_{\mathrm{ColdGas}}}{t_{\mathrm{dyn}}^{\mathrm{gal}}}, \tag{2}$$

where α is a parameter which regulates the efficiency of star formation, M_{ColdGas} is the cold gas mass, and $t_{\mathrm{dyn}}^{\mathrm{gal}} = 0.1R_{\mathrm{vir}}/V_{\mathrm{vir}}$ is the dynamical time of the galaxy, being R_{vir} the virial radius of the halo. Here $\alpha = \alpha_0(V_{\mathrm{vir}}/220\,\mathrm{km\,s^{-1}})^n$, where α_0 and n are free parameters set to 0.1 and 2.2, respectively. Each star formation event generates a stellar mass $\Delta M_{\star}$, which leads to a number η_{CC} of core collapse supernovae (SNe CC). This quantity depends on the initial mass function (IMF) adopted, which in this case is a Salpeter IMF normalized between 0.1 and $100\,\mathrm{M_{\odot}}$; therefore, $\eta_{\mathrm{CC}} = 6.3 \times 10^{-3}\,\mathrm{M_{\odot}^{-1}}$. SNe CC include types Ib/c and II. The energy E_{SNCC} released by each SN CC ($1.2 \times 10^{51}\,\mathrm{erg\,s^{-1}}$) is assumed to reheat the cold gas of a galaxy inducing galactic outflows that transfer cold gas to the hot phase by the amount

$$\Delta M_{\mathrm{reheated}} = \frac{4}{3}\epsilon\frac{\eta_{\mathrm{CC}}E_{\mathrm{SNCC}}}{V_{\mathrm{Vir}}^2}\Delta M_{\star}, \tag{3}$$

where ϵ is a dimensionless parameter which regulates the efficiency of the feedback by SNe CC, and takes a value of $\epsilon = 0.1$. The reheated gas is kept within its host dark matter halo ('retention model', see De Lucia et al. 2004 for other possibilities).

We set an initial primordial abundance of the baryonic components consisting of 76 per cent hydrogen and 24 per cent helium. They become chemically enriched as star formation and metal production take place. Stars contaminate the cold and hot gas as a result of mass losses during their evolution. A fraction f_{ejec} of the mass ejected by galaxies is transferred directly to the hot phase instead of being first incorporated to the cold gas. We adopt here $f_{\mathrm{ejec}} = 0.5$, a value that allows us to obtain an evolution of the mass–metallicity relation consistent with observational data (Erb et al. 2006), resulting in a more gradual contamination of the cold gas associated to each galaxy. The transfer of reheated enriched cold gas also contributes to the chemical enrichment of the hot phase.

Since the cooling rate depends on the metallicity, this chemical enrichment has a strong influence on the amount of hot gas that

can cool. This process in turn influences the star formation activity which is ultimately responsible for the chemical pollution. Thus, new stars formed from the polluted cold gas become more chemically enriched. Stars not only form in a quiescent way from the reservoir of cold gas equation (2) but also from starbursts triggered by mergers and disc instabilities, as we will describe in Section 2.3. The chemical model implemented in our semi-analytic code considers that metals are provided by three kinds of sources: low- and intermediate-mass stars, SNe CC and type Ia supernovae (SNe Ia); the first group of sources yields metals through mass losses and stellar winds (details are given in Cora 2006).

With respect to the spectrophotometric properties of galaxies, we consider evolutionary synthesis models that depend on the metallicity of the cold gas from which stars are formed, estimated for a Salpeter IMF (Bruzual & Charlot 2003). All magnitudes and colours include the effects of dust extinction following the implementation by De Lucia et al. (2004), which is based on previous works (e.g. Kauffmann et al. 1999a).

It is important to remark that SAG1 suppresses gas cooling in rapidly rotating dark haloes ($V_{Vir} > 350 \, \mathrm{km \, s^{-1}}$). This restriction is set with the aim of avoiding very massive and luminous galaxies, thus achieving a better agreement with observations of the bright end of the LF. The reduction or suppression of the cooling flow can be naturally produced by AGN feedback (Bower et al. 2006; Croton et al. 2006). This important physical process is now implemented in the semi-analytic code as we describe in Section 2.4.

2.3 Starbursts in the model: galaxy mergers and disc instabilities

Our new version of the semi-analytic model produces starbursts in three different ways: major mergers, minor mergers and disc instabilities. Starbursts occurring in the last two processes are new ingredients added to the original version SAG1. All the cold gas contained in the galaxies involved in any of these three processes is completely consumed in a sudden burst of star formation.

In a hierarchical scenario of structure formation, mergers of galaxies are a natural consequence of the mergers of dark matter haloes in which they reside, and play an important role in determining the mass and morphology of galaxies. In the subhalo scheme arising from the identification of dark matter substructures, we distinguish three types of galaxies when tracking galaxy formation. The largest subhalo in a FOF group hosts the 'central galaxy' of the group; its position is given by the most bound particle in that subhalo. Central galaxies of other smaller subhaloes contained in a FOF group are referred to as 'halo galaxies'. The (sub)haloes of these satellite galaxies are still intact after falling into larger structures. The third group of galaxies comprises 'satellite' galaxies that arise when two subhaloes merge and the galaxy of the smaller one becomes a satellite of the remnant subhalo. In SAG1, satellite galaxies are assumed to merge on a dynamical time-scale with the central galaxy of the largest subhalo of the FOF group they reside in. It is assumed that the satellite galaxy has a circular orbit with a velocity given by the virial velocity of the parent halo and decays to the corresponding central galaxy through dynamical friction (Binney & Tremaine 1987), given by

$$T_{friction} = \frac{1}{2} \frac{f(\epsilon)}{C} \frac{V_c r_c^2}{G M^{sat} \ln \Lambda}, \tag{4}$$

where M_{sat} is the satellite mass orbiting at a radius r_c inside an isothermal halo of circular velocity V_c. The function $f(\epsilon)$ describes the dependence on the eccentricity of the satellite orbit (see Springel

et al. 2001 for a detailed description), and $C = 0.43$. The function $\ln \Lambda = (1 + M^{central}/M^{sat})$ is the Coulomb logarithm.

Mergers are classified according to the ratio between the mass of the accreted satellite galaxy and the mass of the central galaxy, $f_{merge} = M^{sat}/M^{central}$. A major merger occurs when $f_{merge} > 0.3$; in this case all stars present are rearranged into a spheroid and all the cold gas in the merging galaxies is assumed to undergo a starburst. The stars thus produced are added to the spheroid (bulge). Major mergers constitute a mechanism to produce elliptical galaxies. Subsequent accretion of cooling gas is funnelled into the central galaxy generating a disc.

On the other hand, the merger is classified as a minor merger when one of the two galaxies has a small mass compared to the other, that is, $f_{merge} < 0.3$. Following Malbon et al. (2007), we assume that the presence of a starburst in a minor merger depends on the gas mass fraction of the disc of the central galaxy, $f_{ColdGas}^{central} = M_{ColdGas}^{central}/M_{disc}^{central}$, where $M_{disc} = M_{Stellar} - M_{Bulge} + M_{ColdGas}$. In this last relation, $M_{Stellar}$ is the total stellar mass of the galaxy, M_{Bulge} is the mass of the bulge (formed only by stars), and $M_{ColdGas}$ is the cold gas content of the galaxy. If $f_{ColdGas}^{central} > f_{gas,burst}$, where $f_{gas, burst}$ is a free parameter of the model, the minor merger will produce a starburst as a result of the perturbation introduced by the merging satellite galaxy which drives all the cold gas from both galaxies into the spheroid, where it is completely transformed into stars. Otherwise, if $f_{ColdGas}^{central} < f_{gas, burst}$ then no burst occurs. We adopt a threshold $f_{gas, burst} = 0.6$. Furthermore, if the satellite is much less massive than the central galaxy ($f_{merge} < f_{burst}$, with $f_{burst} = 0.05$, as in Malbon et al. 2007), the central stellar disc remains unchanged and the accreted stars are added to the spheroid; in this case, there is no starburst, regardless of the amount of gas in the central disc, which already contains the contribution of the gas of the satellite.

Starbursts are also triggered by disc instabilities. When a galaxy disc is sufficiently massive that its self-gravity is dominant, it becomes unstable to small perturbations by minor satellites or dark matter substructures (Mo, Mao & White 1998; Cole et al. 2000). We follow the stability criterion from Cole et al. (2000), given by

$$\epsilon = \frac{V_{max}}{(G M_{disc}/r_{disc})^{1/2}}, \tag{5}$$

where V_{max} is the maximum circular velocity of the disc, and M_{disc} is the disc mass. We assume that r_{disc} is the disc-scale radius (following Mo et al. 1998). When $\epsilon < \epsilon_{disc}$ the disc becomes unstable; in the presence of a perturbation all the stars and cold gas in the disc are transferred to the bulge. In this case, all the gas present in this modified bulge is assumed to be consumed in a starburst. After this process, discs are required to stabilize before a new starburst by disc instability can be triggered. We adopt $\epsilon_{disc} = 1.1$ taking into account different observational constraints, as we describe subsequently along the paper. This value lies within the limits given by Mo et al. (1998) (ranging from 0.8 to 1.2) for dark matter haloes with NFW profiles. This mechanism also generates elliptical galaxies.

The upper panel of Fig. 1 shows the evolution with redshift of the number density per unit volume of events that produce starbursts, including major mergers, minor mergers with starbursts, and disc instabilities. As can be seen, starbursts arising from major and minor mergers peak around $z \sim 2$ and 3, respectively. Disc instability events increase in number as the redshift decreases, with a number density that peaks at $z \sim 1$. At lower redshifts, the number of disc instabilities is higher than that of minor mergers. The lower panels of Fig. 1 show the number of events that trigger starbursts weighted by the ratio between the mass of stars produced during the burst and the stellar mass, for galaxies of high stellar mass,
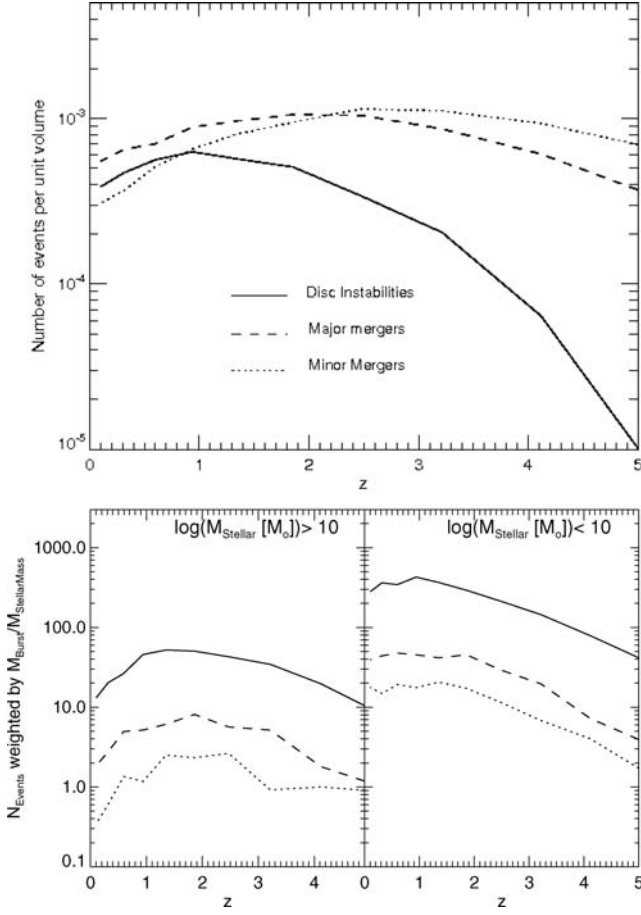
Figure 1. Upper panel: Evolution with redshift of the number density of events that trigger starbursts in our model: major mergers (dashed lines), minor mergers with $f_{gas} > f_{gas, burst}$ (dotted lines) and disc instabilities (solid lines). Lower panels: Evolution with redshift of the number of events weighted by the ratio between the mass of stars produced by the burst and the stellar mass present at the moment of the burst for high (lower left-hand side) and low (lower right-hand side) stellar mass galaxies. Lines are as in the upper panel.

$M_\star > 10^{10}\,\mathrm{M_\odot}$ (lower left-hand panel), and low stellar mass, $M_\star < 10^{10}\,\mathrm{M_\odot}$ (lower right-hand panel). It can be seen that, regardless of the stellar mass, disc instabilities are the preferred mechanism for the growth of stellar mass at all redshifts. Major and minor mergers play a minor role in the growth history of the stellar mass. An important point to notice is that the growth of stellar mass in high-mass systems reaches a peak at redshifts $z \sim 1.5$, whereas low stellar mass galaxies continue to grow almost down to $z = 0$.

2.4 Black hole growth, AGN outflows and gas cooling suppression

As it was discussed before, there is growing evidence that AGN are extremely important for galaxy formation and evolution. AGN are candidates to suppress or reduce cooling flows, thus affecting the star formation process and associated galaxy properties, such as the LF, colours and stellar masses. As it was first pointed out by Hoyle & Fowler (1963), the energy source of a quasar or AGN is gravitational and could arise from a highly collapsed object or a massive BH, an idea broadly agreed to by most authors in the field. Thus, in order to produce AGN, we first need to follow the growth

of central BHs within galaxies, for which we propose a physical model based on a combination of prescriptions given by Croton et al. (2006) and Malbon et al. (2007). Considering that QSOs and AGN are different manifestations of the same phenomenon, the models of BH growth used in these works are motivated by the observational evidence linking the global star formation rate and the optical QSO density in the Universe (e.g. Boyle & Terlevich 1998) in which both are correlated. Given that there are two distinct ways to form stars, either quiescently or in bursts, we also make a difference between the way in which a BH grows in these two modes. We describe these modes separately in the following two subsections.

2.4.1 BH growth in violent star formation processes

We assume that a BH grows from perturbations to the gaseous disc resulting from galaxy mergers or disc instabilities. In such cases, cold gas is funnelled to the centre of the galaxy producing starbursts (Croton et al. 2006). The growth of BHs as a result of these processes is referred to as 'starburst mode growth'. During a galaxy merger, we assume that the central BHs merge instantaneously. For simplicity, we ignore the effects of gravitational waves in BH mergers so that the resulting mass is the direct sum of the two merging masses, with the BH mass in the satellite galaxy being transferred to the BH mass in the central one. The resulting object continues to accrete cold gas. The mass accreted by the BH is proportional to the total cold gas mass present; the efficiency of accretion is lower for unequal mergers. This is summarized by

$$\Delta M_{\mathrm{BH, mer}} = f_{\mathrm{BH}} \frac{M^{\mathrm{sat}}}{M^{\mathrm{central}}} \frac{M_{\mathrm{ColdGas}}}{1 + (200\,\mathrm{km\,s^{-1}}/V_{\mathrm{vir}})^2}, \qquad (6)$$

where M_{ColdGas} is the cold gas mass of the central galaxy after adding the cold gas of the satellite. Note that we use a velocity of $200\,\mathrm{km\,s^{-1}}$ in the above formula instead of a value of $280\,\mathrm{km\,s^{-1}}$ as considered by Croton et al. (2006). As in that work, the value of the parameter f_{BH} is chosen so as to reproduce the observed local relation between the BH mass and the host bulge mass (M_{BH}–M_{bulge} relation), as we discuss in Section 3.2; we adopt $f_{\mathrm{BH}} = 0.015$.

The BH growth through disc instabilities is also represented by equation (6), where the ratio $M^{\mathrm{sat}}/M^{\mathrm{central}}$ is replaced by unity, since this process is a dynamical self-interaction that depends on the properties of a single galaxy. The behaviour of the BH growth during starbursts is shown in Fig. 2, and will be discussed in Section 3.1.

It is important to note that there are no BH seeds in our model and, therefore, the birth of central super massive BHs is triggered when galaxies undergo their first starbursts at some point in their evolution.

2.4.2 BH growth in gas cooling processes

The second way in which BHs are assumed to grow is from cold gas accretion during gas cooling. This occurs once a static hot gas halo has formed around the host galaxy. Note that satellite galaxies do not experiment this growth mode since the reservoir of hot gas is associated only to the central galaxy.

Following Croton et al. (2006), we assume this gas accretion on to the BH to be continuous and quiescent and to be described by a simple phenomenological model,

$$\dot{M}_{\mathrm{BH}} = \kappa_{\mathrm{AGN}} \frac{M_{\mathrm{BH}}}{10^8\,\mathrm{M_\odot}} \frac{f_{\mathrm{hot}}}{0.1} \left(\frac{V_{\mathrm{vir}}}{200\,\mathrm{km\,s^{-1}}} \right)^3. \qquad (7)$$
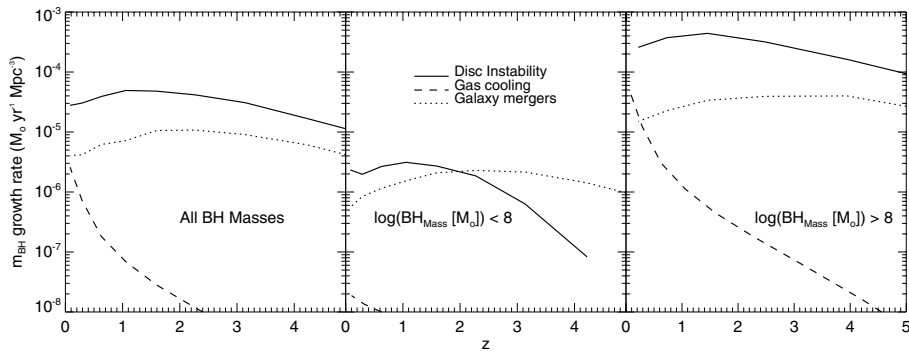
Figure 2. Volume averaged individual BH growth rate as a function of redshift for the three mechanisms that drive the BH growth: gas cooling processes (dashed line), galaxy mergers (dotted line) and disc instabilities (solid line), for all BHs masses (left-hand panel), small BHs ($<10^8$ M$_\odot$, middle panel) and massive BHs ($>10^8$ M$_\odot$, right-hand panel).

In this equation, $\dot{M}_{\rm BH}$ represents the BH accretion rate, $M_{\rm BH}$ is the BH mass, $f_{\rm hot}$ is the fraction of the total halo mass in the form of hot gas, $f_{\rm hot} = m_{\rm HotGas}/M_{\rm vir}$, where $M_{\rm vir}$ is the virial mass of the host halo, and $\kappa_{\rm AGN}$ is a free parameter. Croton et al. (2006) note that $f_{\rm hot}$ becomes approximately constant when $V_{\rm vir} \geq 150\,{\rm km\,s^{-1}}$; the dependence of $\dot{M}_{\rm BH}$ on this quantity is not important.

The mechanical heating generated by the BH accretion (BH luminosity) can be expressed, following the argument of Soltan (1982), as

$$L_{\rm BH} = \eta\,\dot{M}_{\rm BH}c^2, \tag{8}$$

where c is the speed of light, and η is the standard efficiency of energy production that occurs in the vicinity of the event horizon. This process may inject sufficient energy into the surrounding medium to regulate gas cooling since it reduces, or even stops, the cooling flow. Consequently, the cooling rate has to be modified accordingly,

$$\dot{M}'_{\rm cool} = \dot{M}_{\rm cool} - \frac{L_{\rm BH}}{V_{\rm vir}^2/2}. \tag{9}$$

This feedback process is referred to as 'radio mode feedback', following Croton et al. (2006); the way in which BHs grow during this process is thus called 'radio mode growth'.

The BH luminosity depends on the combination of the free parameters $\kappa_{\rm AGN}$ and η (equations 7 and 8, respectively). The local $M_{\rm BH}$–$M_{\rm bulge}$ relation does not help in tuning these values since it is not sensitive to them. However, the QSO and galaxy LFs are good observational constraints. We find that by adopting $\kappa_{\rm AGN} = 2.5 \times 10^{-4}$ M$_\odot$ yr^{-1} and $\eta = 0.1$, the observed shape of the QSO LF and the bright-end break of the galaxy LF are fairly well reproduced as it is described in Sections 3.3 and 3.4.1, respectively.

Notice that we are not taking into account the fact that BHs may be radiatively inefficient when accreting gas during the cooling flow process. This possibility is supported by the presence of BHs at the centre of clusters with cool cores that are usually weak radio sources (e.g. M87 in the Virgo cluster, Le & Becker 2007; Wang et al. 2008). While this particular phenomenon might be accounted for by a non-constant efficiency η, some models use lower BH accretion rates instead (e.g. Jolley & Kuncic 2007; Stern & Poutanen 2008).

2.4.3 Remarks on BH luminosity, $L_{\rm BH}$

The definition of the BH luminosity, $L_{\rm BH}$, given in equation (8), involves the mass accretion rate on to the BH. This quantity is given by equation (7) for the radio mode BH growth. In the case of the starburst mode growth, which occurs during mergers and disc instabilities, the mass accretion rate is estimated from the accreted BH mass in the starburst mode, as it is given by equation (6):

$$\dot{M}_{\rm BH,\,SB} = \frac{\Delta M_{\rm BH,\,accr}}{\Delta T}, \tag{10}$$

where ΔT is the time interval determined by the 50 subdivisions between consecutive simulation snapshots, introduced to increase the accuracy of the integration of differential equations; this is the same time interval applied to estimate $\Delta M_\star$ from equation (2).

In this way, the luminosity of the BH will grow every time the galaxy undergoes star formation in mergers and disc instabilities, and during gas cooling processes with soft, quiescent formation.

2.5 The Eddington limit in the 'BH' luminosity

For a BH of mass $M_{\rm BH}$, the maximum allowed luminosity is the Eddington luminosity, defined as

$$L_{\rm Edd} = 4\pi G M_{\rm BH}\frac{c m_{\rm p}}{\sigma_{\rm T}}, \tag{11}$$

where G is the gravitational constant, $m_{\rm p}$ is the proton mass and $\sigma_{\rm T}$ is the Thompson cross-section for the electron; the latter assumes a gas composed mostly by hydrogen. In this expression, we consider the BH mass at the end of the accretion process. When the calculated BH luminosity is greater than the corresponding $L_{\rm Edd}$, we set $L_{\rm BH} = L_{\rm Edd}$. None the less, we do not limit the BH accreted mass, a choice justified by the lack of strong observational constraints on the efficiency η, that regulates the amount of accreted mass that is transformed into BH luminosity. In our model, the maximum instantaneous fraction of BHs with luminosities over the Eddington limit is only ~6 per cent at very high redshift, so this assumption implies a minor effect.

3 BEHAVIOUR OF THE NEW MODEL SAG2

The principal aim of introducing AGN feedback in models of galaxy formation is to account for the observed influence of AGN on the evolution of galaxies. In particular, the inclusion of AGN in semi-analytic models (Bower et al. 2006; Cattaneo et al. 2006; Croton et al. 2006; Menci et al. 2006; Malbon et al. 2007; Marulli et al. 2008) has also proven to be a good way to avoid problems present in previous versions of semi-analytic models such as an excess of bright, extremely blue galaxies, when compared to observations (as occurs in SAG1).

In the original model SAG1, a number of free parameters was set to regulate the gas cooling, star formation, SN feedback and galaxy mergers, and to determine the circulation of metals among the different baryonic components. These parameters were carefully tuned in Cora (2006) to satisfy numerous observational constraints such as Milky Way properties, the LF, and the TF, colour–magnitude and mass–metallicity relations. An important success of the original code resides in that the implemented chemical model was able to explain the spatial distribution of iron in the intracluster medium at $z = 0$, and the temporal evolution of its mean iron content (Cora et al. 2008).

Once the new free parameters involved in the BH growth and AGN activity are added, a new calibration of the model is performed to reproduce the above mentioned observational constraints plus new observational relationships between the properties of BHs and their host galaxies, that is, BH mass–bulge mass, BH mass–bulge luminosity relations, and the QSO LF.

In the remainder of this section, we analyse the model predictions on BH relations and how the heating of AGN affects galaxy properties.

3.1 Black hole growth

The three different processes driving the BH growth are gas cooling, galaxy mergers and disc instabilities. Their influence on the volume averaged individual BH growth is shown in Fig. 2, represented by different line styles. The left-hand panel involves all BH masses, showing that disc instabilities are the major contributors to the BH growth at all redshifts, closely followed by mergers, both with a smooth variation over a wide range of redshifts. Gas cooling processes become more important at low redshifts with the growth rate steeply increasing by two orders of magnitude for $z \lesssim 2$.

These results differ from those reported by Bower et al. (2006), who find that mergers have a small contribution to the BH growth, and that disc instabilities are the most important contributors at high redshifts. Bower et al. (2006) also find that gas cooling becomes dominant at low redshifts, and that it operates since earlier epochs. On the other hand, Croton et al. (2006) find that the radio mode growth is less important than their 'QSO mode' growth (associated with starbursts) in contrast to the results from Bower et al. (2006), and that it stays constant since $z \sim 2$, a different behaviour to that seen in our model. These differences demonstrate that the model implementation and parametrization have a notorious influence on the detailed history of BH growth. In spite of this, different semi-analytic models are still able to reproduce several observational constraints involving BH masses, such as the 'BH–bulge' relations described in the next subsection.[1]

Fig. 2 also shows the dependence of BH mass growth rate on the three above-mentioned mechanisms for low ($M_{BH} < 10^8 \, M_\odot$, middle panel) and high ($M_{BH} > 10^8 \, M_\odot$, right-hand panel) BH masses. For low-mass BHs, we find that mergers dominate their growth down to $z \sim 2$, where disc instabilities start to dominate for lower redshifts. The effects of gas cooling processes are negligible. In the case of high BH masses, the behaviour of the three mechanisms remains similar to what is shown by the full BH sample.

---

[1] The different BH growth histories presented by these models will show important effects in the global galaxy population at different redshifts. As we show in the remainder of this paper, we use several galaxy statistics to help reduce the degeneracies between semi-analytic models.
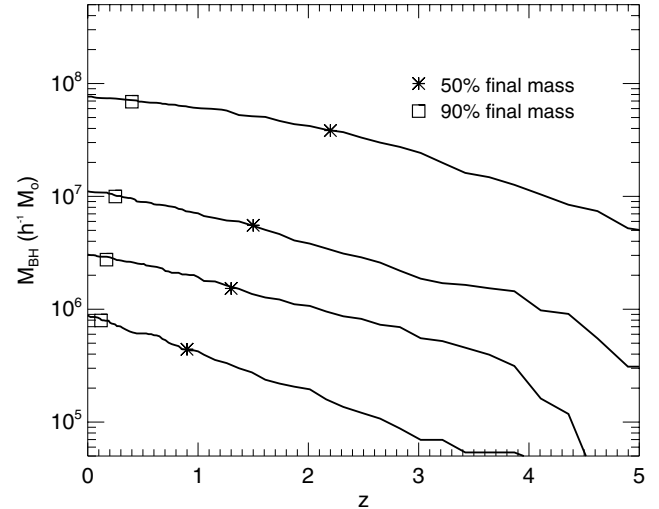

Figure 3. Average growth history of BHs for different mass ranges starting from $z = 5$. The tracks are constructed for a fixed number of BHs per mass bin ordered according to their average masses (lines). The asterisks indicate the points where the BHs have reached half of their final masses, while empty squares represent the time when 90 per cent of the final mass has been accreted.

The average increase of BH mass with redshift for different ranges of BH masses is shown in Fig. 3. High-mass BHs acquire both, half and 90 per cent of their final masses, at earlier times than smaller BHs. In other words, massive BHs form first. This is in agreement with recent observational works (e.g. Marconi et al. 2004) that find that, by $1.5 \lesssim z \lesssim 2.5$, massive BHs have already attained at least one half of their final mass; smaller BHs only reach half of their final mass at $z \lesssim 1$. This is consistent with findings on the evolution of the X-ray LF of QSOs (Cowie et al. 1996; Ueda et al. 2003; Barger et al. 2005), where the number of bright sources is higher at higher redshifts. Moreover, observations have shown that massive galaxies are already in place in the distant Universe (e.g. Drory et al. 2004). With respect to star-forming galaxies, it has been found that their luminosities in the near-infrared bands decline with decreasing redshift since $z \approx 1$ (Cowie et al. 1996). All these observational evidences support the idea of an 'antihierarchical' luminous activity (star formation or mass accretion on to BHs) since it appears to occur earlier in more massive objects, a phenomenon generally termed 'downsizing'.

The evolution of galaxies and BHs are closely connected, as indicated by the BH–bulge relations (Section 3.2). Therefore, the presence of downsizing in the growth of BHs can be understood by taking into account the fact that the star formation activity in massive galaxies peaks at higher redshifts ($z \sim 1.7$) than in less massive objects ($z \sim 0.5$, cf. Fig. 1). This phenomenon is reinforced by the effect of AGN feedback in massive systems that stops the star formation activity earlier, and consequently the fuelling of cold gas that feeds the BHs. Downsizing has also been reported in previous semi-analytic models in the study of both the growth of BH (Bower et al. 2006; Malbon et al. 2007) and of elliptical galaxies (Cattaneo et al. 2008).

3.2 'BH–bulge' relations

We require our model to reproduce as many observational constraints on central BHs as possible. We start by studying the
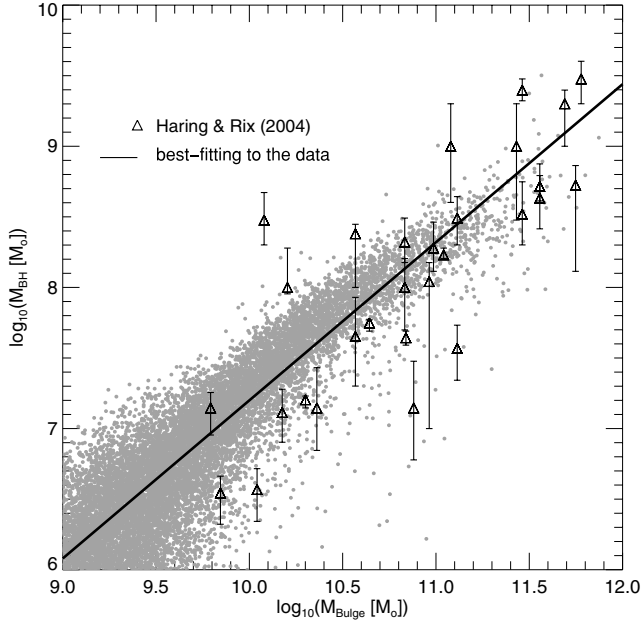
Figure 4. Relation between the BH mass and the host bulge mass. Model results are shown in grey dots. They are compared to observations by Häring & Rix (2004), which are represented by triangles with their corresponding error bars; the solid line corresponds to the best-fitting power law to these data.

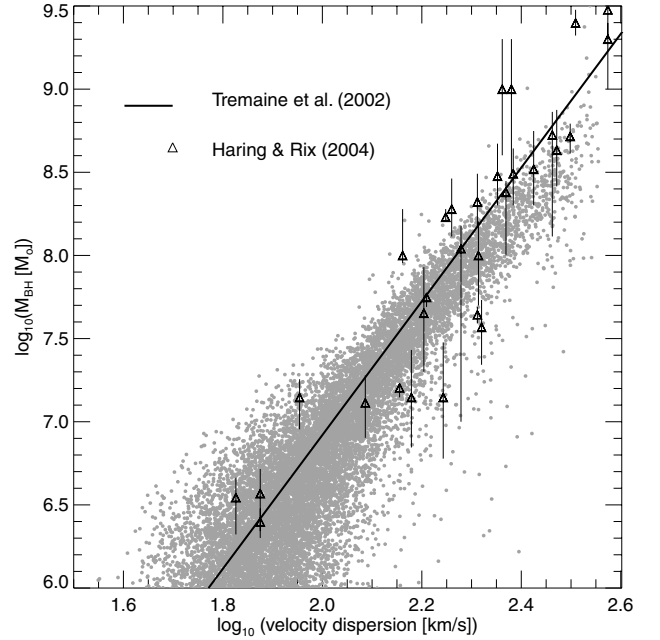relations between the BH mass and the host bulge properties: the 'BH–bulge' relations.

The first comparison, and the most direct one, corresponds to the correlation between BH mass and host bulge mass. In Fig. 4, we compare our model results (grey points) with observations by Häring & Rix (2004), which are shown as triangles, along with their best-fitting power law. In order to obtain a good agreement with this observational relation, we vary the disc instability parameter, $\epsilon_{\rm disc}$, and the parameter $f_{\rm BH}$ (equations 5 and 6, respectively). Even though BHs and bulges grow via the same processes, a well-adjusted correlation cannot be ensured without a fine tuning of these parameters since the BH growth not only depends on the amount of available cold gas, as the bulge growth does, but also on the BH mass and the virial velocity of the halo.

The relations between BH mass and bulge velocity dispersion, $\sigma_{\rm Bulge}$ (Fig. 5), and between BH mass and bulge luminosity (Fig. 6) also show excellent agreement with observations. They are naturally obtained from the choice of model parameters motivated by the BH–bulge mass relation. This agreement is not always reached by other semi-analytic models; for instance, Malbon et al. (2007) show a shallower relation between BH mass and bulge velocity dispersion than the observed trend at high values of velocity dispersion, while our model produces a good match over a larger dynamical range.

3.3 QSO luminosity function

Whenever a BH accretes material there is an associated bolometric luminosity and, therefore, an AGN. Several clues on the nature of AGN are provided by the study of the evolution of the QSO LF.

In order to compare the QSO LF obtained from our model with observational results, we estimate a QSO absolute magnitude in the optical band $M_{\rm bJ}$ (blue magnitude in Johnson's system), following

Figure 5. Relation between the BH mass and host bulge velocity dispersion, $\sigma_{\rm Bulge}$. Model results are represented by grey points. They are compared with observations of Häring & Rix (2004) (triangles) and Tremaine (2002) (solid line).
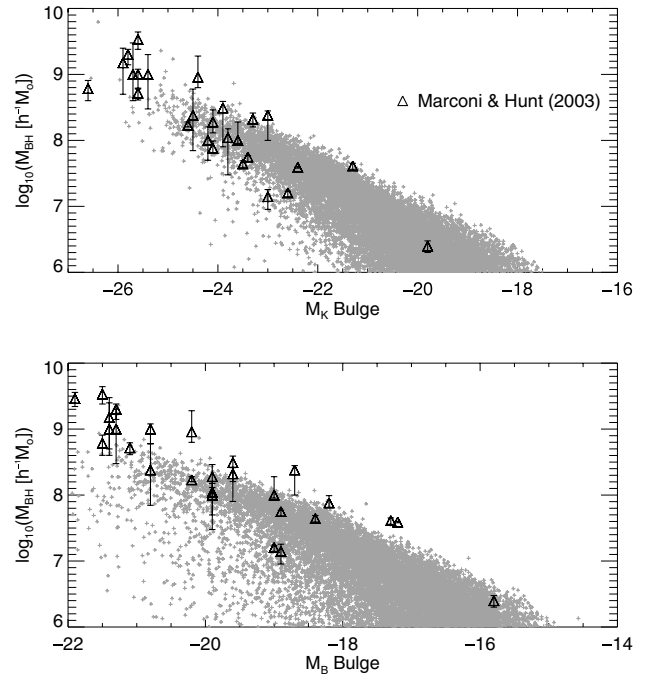

Figure 6. Relation between the BH mass and bulge *B*- and *K*-band absolute magnitudes. Model results are represented by grey points [compared with observations of Marconi & Hunt (2003) (black triangles)].

equation (12) of Croom et al. (2005):

$$M_{\rm bJ} = -2.66 \log_{10}(L_{\rm Bolom}^{\rm QSO}) + 79.42, \tag{12}$$

where $L_{\rm Bolom}^{\rm QSO}$ is the bolometric luminosity in units of watts given by the BH luminosity defined by equation (8). We then build the QSO LF at different redshifts and compare its evolution with measurements by Croom et al. (2004) and Wolf et al. (2003). The former
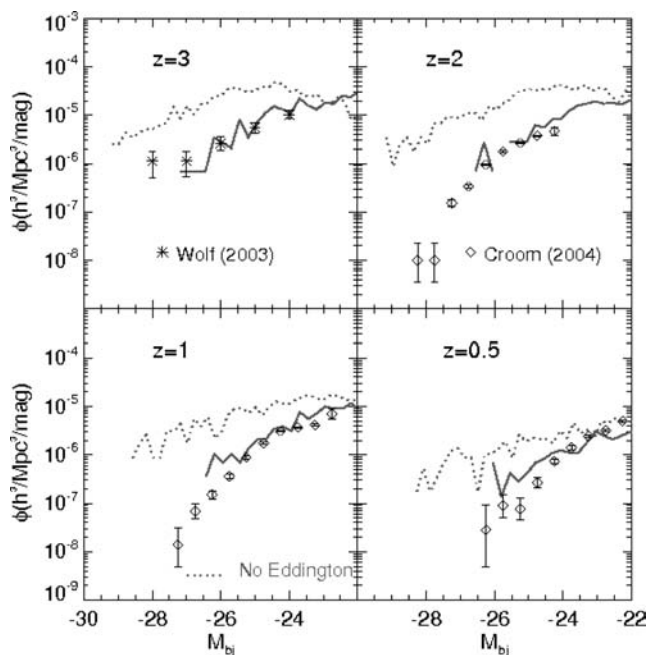
Figure 7. Model QSO LF compared with observational data by Croom et al. (2004) for $z \lesssim 2$, and Wolf et al. (2003) at $z \approx 3$. The grey solid lines show the final model including Eddington limit with the parameters indicated in Section 2. To obtain good agreement with observations it was necessary to assume a fraction, $f_{\mathrm{obsc}} = 0.8$ of obscured QSOs. The resulting model QSO LF with no Eddington limit is represented by grey dotted lines.

work presents results for the QSO LF from the 2dF QSO redshift survey (2QZ) over the redshift range $0.4 \lesssim z \lesssim 2.1$, while the latter uses the COMBO-17 survey that contains a large sample of faint QSOs in the redshift range $1.2 \lesssim z \lesssim 4.8$. Note that the LF found by Wolf et al. (2003) is consistent with results obtained from surveys such as SDSS and 2QZ.

The QSO LF is shown in Fig. 7. The results of our model (solid lines) are in good agreement with the observational data of Wolf et al. (2003) and Croom et al. (2004), represented by symbols. These results are obtained by the inclusion of the Eddington limit (Section 2.5) and a fraction of obscured QSOs. The application of the Eddington limit helps to recover the observed QSO LF, although a constant normalization offset remains at all redshifts. In order to solve this discrepancy, we find important to consider that a fraction f_{obsc} of model QSOs are obscured by the gas torus assumed to be present in the 'unified model' of AGN galaxies (e.g. Fanaroff & Riley 1974; Barthel 1989; Madau, Ghisellini & Fabian 1994; Gunn & Shanks 1999); we adopt $f_{\mathrm{obsc}} = 0.8$. This fraction is consistent with observational results (Gunn & Shanks 1999; Lacy et al. 2007) which show that a large number (possibly the majority) of QSOs are obscured.

Model results with $f_{\mathrm{obsc}} = 0.8$ and no Eddington limit are represented as grey dotted lines, showing that this limit produces changes up to a factor of $\sim$6 in the QSO luminosity. Malbon et al. (2007) also find that the Eddington limit contributes to obtain a good agreement with observations. We remark that our simulation box size is only mid-size and, therefore, does not allow us to reproduce the entire dynamic range of observed QSO number densities.

We stress the fact that we are using a fixed value of f_{obsc} at all redshifts; therefore, it can be said that QSO luminosities in our model depend exclusively on the physical properties of the AGN phenomenon. We notice, however, that at low redshifts the

model shows slightly higher number densities than the data, possibly implying a larger obscured fraction as the redshift decreases. There is some observational evidence in this direction, where the fraction of obscured QSOs becomes higher at $z \lesssim 1$ (e.g. Franceschini, Braito & Fadda 2002; Gandhi & Fabian 2003). However, this redshift dependence is not always found (e.g. Gilli 2004; Ueda et al. 2003), being necessary larger samples to understand this trend. On the other hand, the results obtained by Ueda et al. (2003) imply that the fraction of absorbed AGN decreases at high luminosities. Our model shows the opposite behaviour; a larger fraction of obscured AGN is required at the bright end of the LF to further improve the agreement with the observational data.

As we have mentioned in Section 2.4.2, the shape of the QSO LF is sensitive to the parameter κ_{AGN}, responsible for the regulation of the gas accretion rate on to BHs via gas cooling processes. Adopting larger values of κ_{AGN} leads to a higher QSO number density. This increment occurs at high redshifts ($z \gtrsim 1$) for low and intermediate luminosities, while at lower redshifts it mainly affects the bright end of the QSO LF. The latter arises as a consequence of the increased impact of gas cooling processes on the growth of massive BHs at low redshifts. It is important to remark that we do not make assumptions about the QSO lifetime since we consider the BH luminosity as the instantaneous rate of energy ejected from the BH.

### 3.4 Galaxy properties: effects of AGN feedback

Semi-analytic models are calibrated to reproduce, as best as possible, properties of galaxies in the local Universe such as the LF, the TF relation, colour–magnitude diagram and gas fractions. The LFs in different colour bands obtained from SAG1 are characterized by an excess of bright galaxies with respect to the observed LFs. The TF relation is found to lie within the observational error determinations, following the best-fitting estimation by Giovanelli et al. (1997). The colour–magnitude relation for early-type galaxies managed a very good agreement with the observational fitting by Bower, Lucey & Ellis (1992). Gas fractions were also found to be in very good agreement with observational results by McGaugh & de Blok (1997).

In this section, we analyse the advantages of the new model SAG2 which now includes AGN feedback, evaluating the influence of this process on different galaxy properties, and comparing with the results provided by the original version SAG1.

3.4.1 Luminosity and stellar mass functions

LFs in the b_{J} and K bands are shown for SAG2 galaxies in Fig. 8. It can be seen that in both cases the model closely follows the trend denoted by the observational results from Norberg et al. (2002) for the b_{J} band, and Huang et al. (2003) and Cole et al. (2001) for the K band. At the bright end of the LF, the agreement with observations has improved significantly over the previous version of the model, SAG1. This improvement comes from a more vigorous quenching of cooling of hot gas at low redshifts operating in SAG2, which prevents the presence of very luminous massive galaxies.

The masses of model galaxies are able to reproduce the observed evolution of the stellar mass function (SMF). The dependence of the SMF with redshift is shown in Fig. 9. Here we compare the SMF from our model SAG2 with observations from Drory et al. (2004) and Drory et al. (2005) in four redshift bins, from $z \simeq 0.5$ to 4.5; model results are represented by black solid lines. The model SMF is in good agreement with observations at all redshifts. The grey
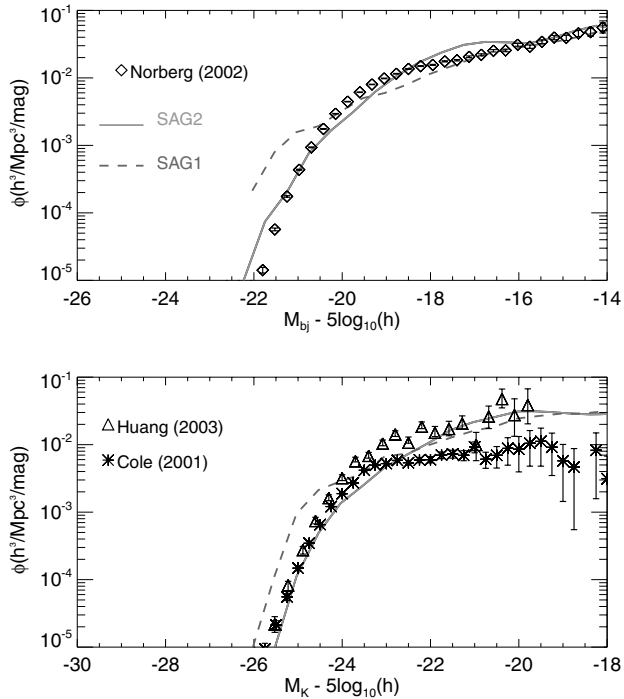
Figure 8. Upper panel: b_J-band galaxy LF. Lower-panel: K-band galaxy LF. Solid lines represent results from our new model, SAG2, while dashed lines correspond to the previous version, SAG1; different symbols identify observational LF estimates by Norberg et al. (2002), Huang et al. (2003) and Cole et al. (2001).
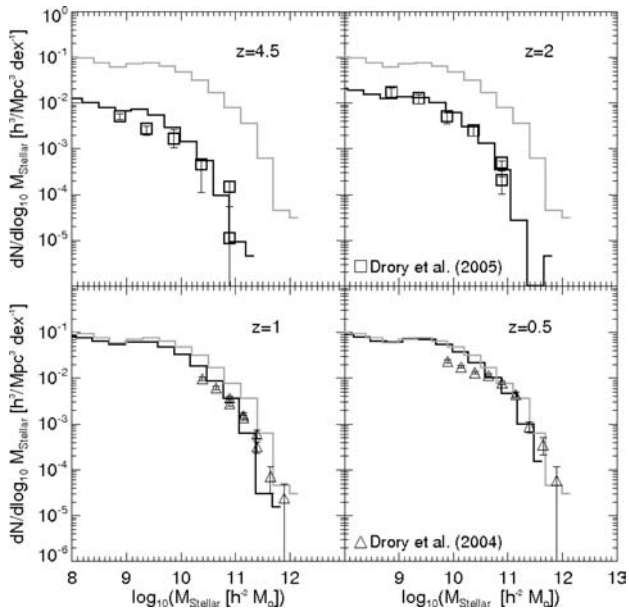
Figure 9. SMF for the model galaxies in SAG2 at redshifts $z = 4.5, 2, 1$ and 0.5 (black solid lines); for comparison, all panels show the $z = 0$ model SMF (grey solid lines). Symbols represent observational data from Drory et al. (2004) and Drory et al. (2005).

lines show the $z = 0$ model SMF, and help to illustrate the lack of significant evolution in the SMF from $z \sim 0.5$.

Note that our model uses a Salpeter IMF; certain models consider different IMFs (e.g. Baugh et al. 2004 use a top-heavy IMF) in order to reproduce the observational results. It is important to remark that Drory et al. (2004) and Drory et al. (2005) also assumed a Salpeter

IMF to apply photometric techniques to determine redshifts and stellar masses of the best-fitting templates of galaxy spectra. They also analyse two independent fields, the FORS deep field and the GOODS-S field, implying that the data take into account cosmic variance to some degree and are therefore representative of the observed Universe at low and high redshifts.

3.4.2 Galaxy morphology

We analyse the morphology of SAG2 galaxies at $z = 0$. In order to determine a fraction of morphological types from the model, we use the ratio between the bulge mass and the total stellar mass, $r = M_{Bulge}/M_\star$, as proposed by Bertone, De Lucia & Thomas (2007) for this type of analysis. We adopt a threshold between ellipticals and spirals $r_{thres} = 0.95$, classifying as ellipticals all bulge-dominated systems with $r > r_{thres}$, and as spirals those with $0 < r < r_{thres}$; systems with no bulge ($r = 0$) are classified as irregulars. The threshold between ellipticals and spirals is not firmly established; for instance, Bertone et al. (2007) use $r_{thres} = 0.7$. None the less, a higher threshold, as the one adopted here, defines very well the elliptical population, allowing them to have at the most a stellar disc of 5 per cent the total mass.

Fig. 10 shows the fractions of morphological types as a function of stellar mass for our model (represented by lines) and the observational data by Conselice (2006), represented by symbols with error bars. The data include a sample of more than 22 000 galaxies at $z \lesssim 0.05$ with a visual morphological classification from the RC3 catalogue (de Vaucourleurs 1991b). We can appreciate that the fractions of different morphological types in the model agree very well with the observations over the whole stellar mass range. SAG2 shows a clear improvement over the previous version of our model, SAG1, in which $\sim$80 per cent of massive galaxies evolved to be spirals. Starbursts triggered by disc instabilities are a key ingredient to
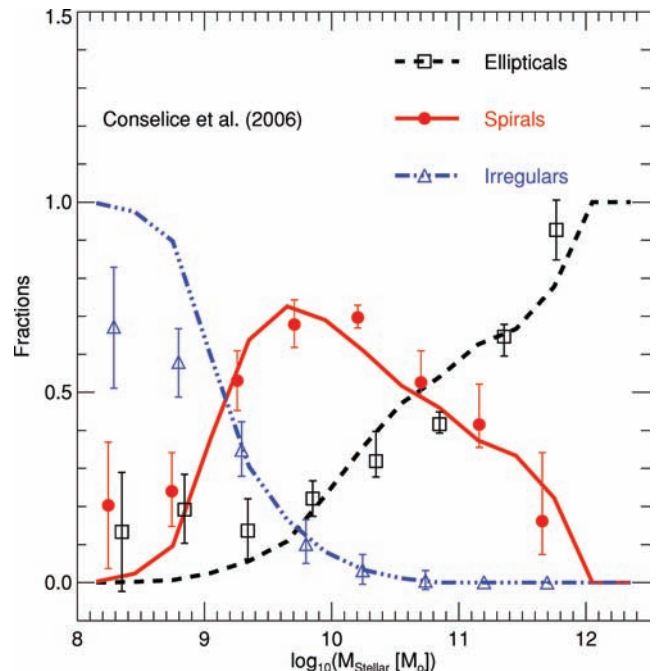
Figure 10. Fractions of SAG2 galaxies of different morphological types at $z = 0$ as a function of stellar masses. Model results (lines) are compared with observations taken from Conselice (2006) (symbols): irregular galaxies are represented by dash–dotted lines and triangles, spirals by solid lines and filled circles, and ellipticals by dashed lines and open squares.

achieve a good agreement with the observed morphological types; disc structures are destroyed during these events thus favouring the formation of early-type galaxies. When including disc instabilities in SAG1 the percentage of high stellar mass spirals is reduced to ~40 per cent.

Changes in r_{thres}, which we varied from 0.7 and 0.95, produce a shift in the height of the spiral fraction peak from ≃0.55 to ≃0.75. Spiral galaxies at intermediate stellar masses are the more sensitive population to r_{thres}. Elliptical galaxies are the dominant type at high stellar masses regardless of the value of this parameter.

In order to test the reliability of the morphological classification described above, we apply the criteria given by De Lucia et al. (2004), in which spiral galaxies satisfy the condition $1.2 < M_{B,Bulge} - M_{B,Gal} < 2.4$; we also consider the definition of Hubble types given by Springel et al. (2001). Our conclusions are not significantly affected in any of these cases.

Recent works on the analysis of morphological types in semi-analytic galaxies obtain slightly different results. De Lucia & Blaizot (2007) fail to predict the presence of high-mass spiral galaxies. On the other hand, Bertone et al. (2007) show a good agreement with observations at all stellar masses although their model produces a significant excess of bright galaxies in the LF and a smooth colour distribution with most of their galaxies residing in a red sequence. The morphological aspect of model galaxies is quite sensitive to the different parametrizations of the processes affecting the star formation, including the effects of disc instabilities and major and minor mergers. Thus, it is not surprising that different semi-analytic codes lead to different dependencies of morphological type fractions with stellar mass.

3.4.3 Galaxy colours

The AGN feedback has an important effect on galaxy colours. Fig. 11 presents $B - V$ colours as a function of stellar mass for the models SAG1 (left-hand panel) and SAG2 (middle panel), where galaxies are separated in ellipticals (red symbols) and spirals (blue symbols) following the criteria outlined in Section 3.4.2. The right-hand panel shows the same SAG2 galaxy population splitted into central (black symbols) and satellite galaxies (green symbols).

SAG2 galaxies show that the inclusion of AGN feedback produces galaxies with $B - V$ colours qualitatively compatible with measured colour distributions (see e.g. Baldry et al. 2006) including a bimodal behaviour and a negligible population of massive ($\gtrsim 10^{11} h^{-1} M_\odot$) blue galaxies. This is a clear difference with respect to SAG1 where there is a population of very massive, blue spiral galaxies. As it was mentioned in Section 3.4.2, this is a consequence of the genera-

tion of new spheroids by the action of the disc instability process included in SAG2.

The right-hand panel of Fig. 11 indicates that the red branch is mainly composed by satellite galaxies, characterized by the fact that their hot gas reservoir has been stripped when they were accreted by the central halo, aging quiescently until merging with a central galaxy. Massive central galaxies also become red as a result of a combination of different effects. On the one hand, the reduction or suppression of gas cooling leaves a galaxy with a limited cold gas reservoir that is eventually exhausted; it then undergoes a passive evolution unless a merger with another galaxy takes place. However, the possibility that this occurs decreases at low redshifts, as it is shown in Fig. 1. On the other hand, if a merger occurs, it is very unlikely that satellite galaxies will contribute enough cold gas to produce a starburst that will appreciably change the colour and mass content of the central galaxy, since the gas cooling process does not occur in satellites. Hence, mergers would more likely only increase the mass of the stellar population without giving place to an important generation of new stars.

4 FURTHER IMPROVEMENTS TO THE SEMI-ANALYTIC MODEL OF GALAXY FORMATION

In this section, we explore the effects of two new ingredients that can be added to the model. We first take into account an additional form of feedback from AGN, associated with the BH growth during starbursts. Then, we focus on the analysis of the effects of different prescriptions for the dynamical friction time-scales affecting galaxy mergers.

4.1 AGN feedback in starburst events

The importance of AGN feedback in galaxy evolution is undeniable, as theoretical and observational works indicate, although this is still a poorly understood phenomenon and is at present a matter of debate. It is mostly accepted that the quiescent gas accretion produces feedback from the active nucleus, but there is no general consensus on the fate of the energy produced by the BH mass accretion during starbursts. Therefore, in this section, we use our new semi-analytic model SAG2 to explore the effects of AGN feedback during violent events (i.e. starbursts) on galaxy properties.

There are observational clues about the influence of AGN feedback in starbursts. Donahue et al. (2005) propose a dichotomy in galaxy clusters between those which are radio active and show strong central temperature gradients (indicating the action of AGN
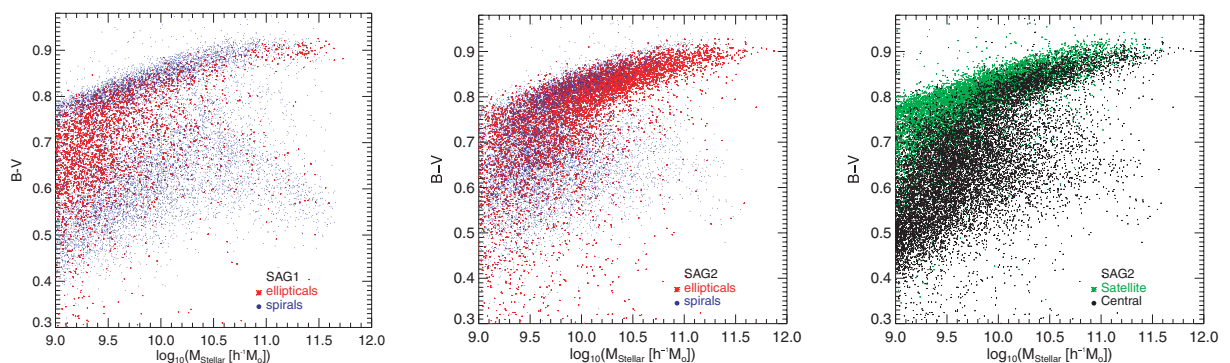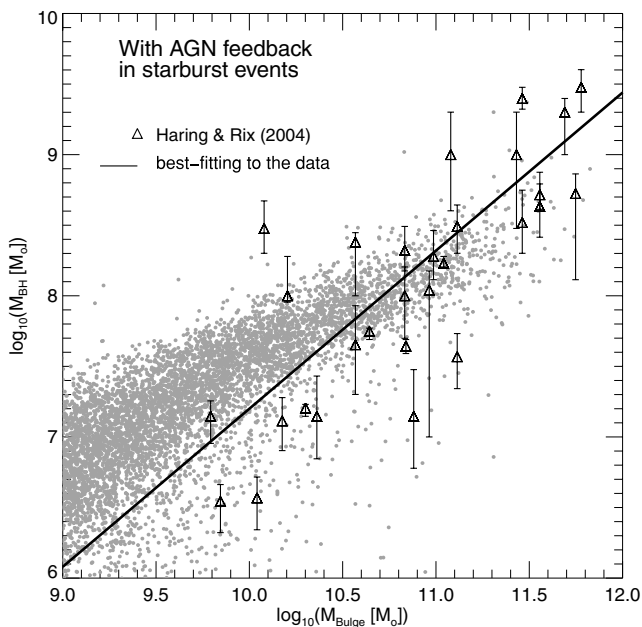

Figure 11. Colour distribution for ellipticals (red symbols) and spirals (blue symbols) type galaxies obtained from models SAG1 (left-hand panel), and SAG2 (middle panel). SAG2 galaxies separated into centrals and satellites are also shown (right-hand panel, black and green symbols, respectively).
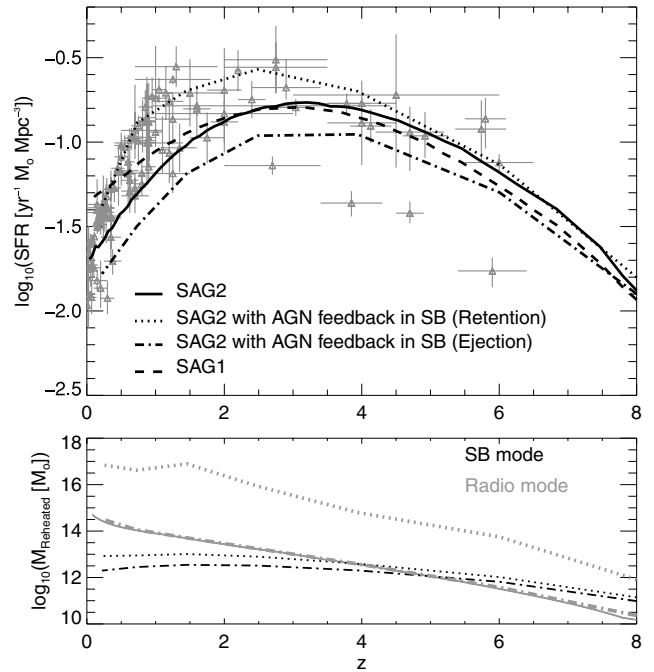
feedback), and radio-quiet with no temperature gradients. None the less, Gastadello et al. (2007) find a counter-example in the cluster AWM 4 characterized by the absence of a temperature gradient, as indicated by the *XMM* data, and the presence of an active radio source at 1.4 GHz. The combination of these features cannot be explained if AGN activity is regulated only by feedback from gas cooling processes.

We explore the effects of AGN feedback during starbursts following two different possibilities: (i) the outflowing material is directly transferred to the hot gas surrounding galaxy and (ii) the energy produced is high enough to expel material out from the galaxy halo without affecting any baryonic component associated to the galaxy. We refer to these two mechanisms as retention and ejection modes, respectively; the former has been used in both SNe feedback and AGN feedback in radio mode throughout this work. The absence of definitive evidence favouring one scenario or the other only allows us to analyse and compare the outcomes from each option. Note that the ejection mode does not operate exactly in the same way as in, for example, De Lucia et al. (2004), where the ejected gas is eventually reincorporated to the dark halo. AGN feedback in starburst mode heats the cold gas already present in the galaxy with a rate $2L_{BH}/V_{Vir}^2$. The BH luminosity, L_{BH}, given by equation (9), now involves the mass accreted in the starburst mode, as given by equation (10).

Fig. 12 shows the relation between BH and bulge masses considering AGN feedback produced when the accretion occurs as a result of starburst events, for the case of the ejection mode. The results from the retention mode are not shown in this figure since the general trend does not vary appreciably with respect to the ejection scenario, and only produces a larger scatter of BH masses. As can be seen, AGN feedback during starbursts produces only slight changes with respect to the model where only radio mode AGN feedback is applied (see Fig. 4). The main difference is a shallower relation produced by the complementary effect of AGN feedback in starbursts, which reduces even more the available cold gas for bulge growth so that, for small BHs, bulge masses are smaller. Note

Figure 13. Upper panel: Cosmic star formation rate for SAG2 (solid line), SAG2 including AGN feedback during starburst (with the same parametrization as SAG2; dotted and dot–dashed lines for the retention and ejection modes, respectively) and SAG1 (dashed line), compared to observations compiled by Hopkins et al. (2006) (grey triangles with error bars). Lower panel: Reheated mass from the different feedback mechanisms as a function of redshift for the different AGN feedback models. The grey lines represent the radio mode and the black lines the starburst mode.

Figure 12. Relation between BH and bulge masses for model results including AGN feedback during starbursts in the ejection mode (grey points) compared with observational estimates by Häring & Rix (2004) (triangles).
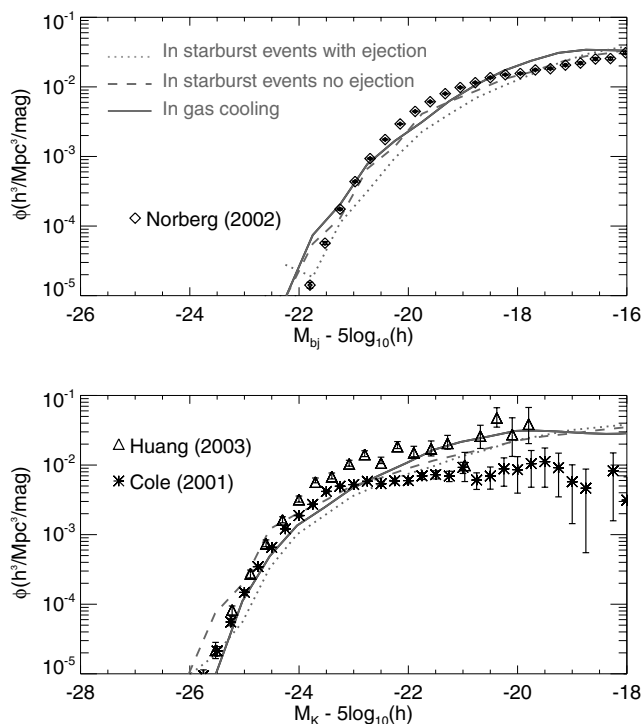
that this does not affect BH masses as significantly since BHs grow mainly through mergers and disc instabilities (cf. Fig. 2). In any case, the poor statistics in the observational relation does not allow us to determine which of the three versions of our model (AGN feedback from gas cooling, or AGN feedback during starbursts for the retention/ejection mode) provides the best agreement.

We have to take into account that AGN feedback in starburst mode is an additional ingredient that changes the mass and metallicity of the hot gas, which in turn affects the cooling rate and thus the stellar formation rates. Fig. 13 shows the global cosmic star formation rate as a function of redshift for the models SAG1 (dashed line), SAG2 (solid line) and SAG2 including AGN feedback in starbursts for the retention (dotted line) and ejection (dot–dashed line) modes. The latter two models use the same set of parameters as SAG2. Comparing SAG2 with SAG1, we can appreciate that, for $z \gtrsim 3$, the SFR is larger in SAG2 as a result of the disc instability and starbursts in minor mergers included in this model. The feedback in radio mode becomes progressively more effective for lower redshifts, increasing the reheated mass (solid grey line in lower panel of Fig. 13) and appreciably reducing the SFR. When including AGN feedback in starbursts in the ejection mode, the SFR is reduced at all redshift both with respect to SAG1 and SAG2, keeping the similar redshift dependence as in SAG2. This is a consequence of the removal of gas by the ejection mode, which is no longer available to cool and form stars. In the case of the retention mode for the AGN feedback in starbursts, the gas is mainly reheated by the radio mode, as shown in the lower panel of Fig. 13. This is due to a larger reservoir of hot gas available for gas cooling due to the retention of the gas heated by the AGN. This produces a much

higher SFR in this mode with respect to the other models shown in the figure.

Three models, SAG1, SAG2 and SAG2, with retention mode AGN feedback in starbursts, show a reasonable agreement with the observational data compiled by Hopkins et al. (2006) (grey symbols with error bars) at all redshifts. However, SAG1 results show a too high SFR at $z = 0$. On the other hand, SAG2 with AGN feedback in starbursts in the ejection mode, shows a much lower star formation history (SFH) at all redshifts, although it should be noticed that some observational data points are consistent with even lower values of SFR at $z \gtrsim 2$. Note that SAG2 provides a good agreement with the observed SFH at all redshifts. Only at $z \simeq 1$ the model shows slightly lower values than the distribution of observational results. However, recent studies by Wilkins, Trentham & Hopkins (2008) show that direct measurements of star formation rates (e.g. Hopkins et al. 2006) seem to be overestimated with respect to the SFR values obtained from SMFs. Taking this into account, the agreement between our model SAG2 and observations at $z \simeq 1$ would be even more consistent.

We also analyse how the inclusion of AGN feedback in starburst mode affects the galaxy LF. Fig. 14 shows the b_J-band (top panel) and K-band (bottom panel) LFs for the three different models: SAG2 (solid line), SAG2 including feedback in starbursts in the retention (dashed line) and ejection modes (dotted line). As can be seen in Fig. 13, SAG2 gives lower SFRs when AGN feedback in starbursts with ejection is included. Therefore, in this case the LF is slightly shifted towards fainter luminosities by up to half a magnitude. As the agreement with observed results is not badly affected by this, we do not need to recalibrate the model parameters in this

case. In the retention mode, the radio mode feedback efficiency, the κ_{AGN} parameter equation (7), needs to be increased in order to reproduce the observed bright end of the LFs; we adopt $\kappa_{AGN} = 2 \times 10^{-3}\,M_\odot\,yr^{-1}$. After applying this recalibration, the retention mode produces a good agreement with observations.

The morphology of model galaxies (estimated as in Section 3.4.2) is affected by the AGN feedback during starbursts. The ejection mode improves the agreement with the observed morphological fractions at low stellar masses (Conselice 2006), producing a non-zero spiral population at this mass range. This mode also maintains the good agreement at intermediate and high stellar masses shown by SAG2. On the other hand, the retention mode fails to reproduce the observed morphological fractions at all masses, even after the feedback efficiency, κ_{AGN}, is increased in order to match the observed galaxy LF.

The failure of the retention mode can be used as an indication that, if present, AGN feedback during starbursts should be strong enough to expel the reheated material away from the galaxy halo. The only drawback to this ejection model is that it may produce slightly low values for the SFH with respect to the observational trend, which in any case still shows data points that lie below the model prediction at high, $z > 2$, redshifts.
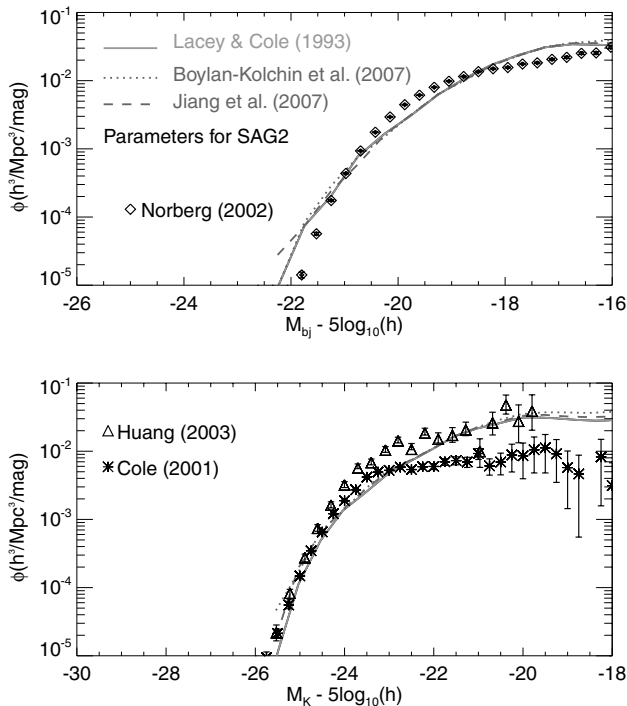
The implementation of AGN feedback in starbursts is still crude since it considers the same efficiency as in the AGN feedback acting during gas cooling. It is possible though, that the physical considerations needed for these two different accretion processes, via gas cooling and during starbursts, are not the same. For instance, instead of using different BHs feeding mechanisms to distinguish between different feedback modes, the model described by Sijacki et al. (2007) uses a threshold value for BH accretion rate above of which the feedback is similar to our starburst mode although with a lower efficiency. We leave the detailed study of AGN feedback during starbursts to a forthcoming paper.

4.2 New prescriptions for merger time-scales

All the results presented in this work have been obtained considering that galaxy mergers are driven by the dynamical friction process, for which we have adopted the prescription given by Lacey & Cole (1993, hereafter LC93). We now take into account the new dynamical friction time-scales proposed by Jiang et al. (2007) and Boylan-Kolchin et al. (2007) (hereafter J07 and B07, respectively). Both studies use numerical simulations to measure merger time-scales and compare them to theoretical predictions based on the Chandrasekhar formula. They find that, in contrast to Navarro, Frenk & White (1997), the theoretical merger time-scales are not in agreement with the simulated values. Equation (5) from J07 and equation (5) from B07 provide new fittings to the merger time-scales that we test in our model. The difference between these two fittings resides in the weaker dependence on circularity in the prescription of J07 compared with the one by B07. The overall conclusions from both studies are the same, that the LC93 merger time-scales are underestimated for minor mergers and overestimated for major mergers.

The effects of the three different merger time-scales on the galaxy population can be readily seen in Fig. 15, where we show the LF in the b_J and K bands (upper and lower panels, respectively; using the SAG2 parameter set) for the three different approximations. The three models are in good agreement with observations in both bands.

Changing the merger time-scales according to the new prescriptions of J07 and B07 produces a decrease in the merger frequencies. Both major and minor mergers are affected, although the changes

Figure 14. b_J-band (upper panel) and K-band (lower panel) LFs for three models: when AGN feedback is acting only during gas cooling process (solid line), when AGN feedback is also produced in starburst events with ejection of the reheated material (dotted line); and when the material is retained in the dark halo in which the galaxy resides (dashed line). In the ejection mode we use the same set of parameters as in SAG2, while a value of $\kappa_{AGN} = 2 \times 10^{-3}\,M_\odot\,yr^{-1}$ is adopted in the retention mode.

Figure 15. b_J and *K* bands galaxy LF for three different merger time-scales; the results using the prescription by LC93 are shown by solid lines, those from J07 and B07 are represented by dashed and dotted lines, respectively.

are more important for the minor mergers. This translates into a shift in the period of maximum merger activity towards redshifts closer to $z \sim 1.5$, much lower than that obtained for LC93, which occurs at $z \sim 2.5$. In turn, this affects the disc instability frequency presented in Fig. 1 producing an order of magnitude increase in the number of events. This is a result of the longer time-scales over which galaxies can form stars and accrete gas into the disc. The higher number of disc instabilities and the delayed action of mergers compensate each other, and no recalibration of the model parameters is needed in order to obtain a good agreement between model and observational galaxy properties such as the $z = 0$ galaxy LF and bimodal galaxy colour distributions, stellar masses at different redshifts, 'BH–bulge' relations, and the SFH.

The new time-scales affect galaxy morphologies producing a 10 per cent excess of elliptical galaxies at intermediate stellar masses with respect to observations (e.g. Conselice 2006). A possible reason for this slight excess of spheroids is that the frequency of disc instability events increases producing a somewhat larger population of smaller elliptical galaxies than SAG2 and the observations. At the high-mass end, the J07 prescription produces a slightly better agreement with the observed morphological fractions.

As it was mentioned above, the effect of the new merger time-scales is difficult to detect in the galaxy statistics studied in this paper. However, the study of quantities that are affected by the detailed stellar mass growth may show more important differences, as would probably be the case for the amount of stellar mass formed in accreted satellites.

5 SUMMARY AND CONCLUSIONS

As several recent observational results indicate, AGN feedback has become a very important element in our understanding on galaxy evolution (e.g. Nulsen et al. 2007; Schawinski et al. 2007). In this

paper, we study the effects of AGN feedback on the formation and evolution of galaxies by using a combination of a cosmological *N*-body simulation of the concordance ΛCDM cosmology and a semi-analytic model of galaxy formation. We have developed an AGN feedback model based on different implementations considered in recent semi-analytic models (Bower et al. 2006; Croton et al. 2006 and Malbon et al. 2007), which are based on both, observations and a phenomenological picture of the physics governing the extremely massive, central BHs, and of the gas ejected by these central engines back to the interstellar or even the intergalactic medium. Our semi-analytic model is an improvement of the one described by Cora (2006) which involves gas cooling, star formation, galaxy mergers and SN feedback, with the advantage of including a proper treatment of the chemical enrichment of baryons. The new version of this model (SAG2) benefits from the inclusion of AGN feedback. In our model, the AGN activity is triggered by the accretion of cold gas on to BHs, which grow via three distinct channels: (i) mergers between two pre-existing BHs, (ii) mass accretion during gas cooling processes and (iii) gas accretion during starbursts. The latter are produced during major and minor mergers, and disc instabilities, being the last two processes new ingredients to our model. BHs produce a luminosity which is proportional to the gas accretion rate. When the accretion is produced during the gas cooling process, the resulting AGN produces feedback (radio mode feedback). It is also considered the possibility that AGN generated by the BH growth during starbursts also produce feedback. Another novel feature analysed in our model is the influence of new prescriptions for merger time-scales on galaxy properties.

We summarize the main results of this work.

(i) The growth history of galaxies is dominated by both major mergers and disc instabilities, while minor mergers play only a minor role (Fig. 1). The frequency of starbursts peaks between $z \sim 2$ and 3 when produced by mergers, and between $z \sim 1$ when produced by disc instabilities.

(ii) The accretion history of BHs shows small variations between high- and low-mass BHs. For high-mass BHs at $z = 0$, $M_{BH}(z = 0) > 10^8 \, M_\odot$, the accretion is dominated by disc instabilities at all redshifts. Instead, mergers dominate at $z \gtrsim 2$ for lower masses, with a larger influence of disc instabilities at lower redshifts (Fig. 2). Regardless of the BH mass, the accretion via gas cooling processes is negligible. Higher mass BHs assemble earlier in the history of the universe (Fig. 3), in agreement with the downsizing scenario (e.g. Marconi et al. 2004; Shankar et al. 2004).

(iii) We simultaneously obtain good agreement with observations in several 'BH–bulge' relations: BH–bulge mass (Fig. 4), BH mass as a function of bulge velocity dispersion (Fig. 5) and bulge luminosity (Fig. 6); these agreements were achieved using a fixed value of the parameter f_{BH} equation (6) tuned to match the observed BH–bulge mass relation.

(iv) Our model predicts that a large fraction (80 per cent) of model QSOs need to be obscured in order to reproduce the observed QSO LF (Fig. 7). Many studies have indicated this fact but fail to provide accurate estimates of this fraction (e.g. Gunn & Shanks 1999; Lacy et al. 2007). At low redshifts the model shows slightly higher QSO number densities than the data, indicating the possibility that the obscured fraction needs to become larger as the redshift decreases, as suggested by some observational results (e.g. Franceschini et al. 2002; Gandhi & Fabian 2003).

(v) SAG2 reproduces many of the observed properties of the local galaxy population that were also reproduced by the previous version of the model (e.g. the TF relation, and the relation between gas

fraction and absolute M_B magnitudes). The observed bright end of the galaxy LFs in the b_J and K bands (Fig. 8) have been successfully recovered by sag2 galaxies, being one of the main successes of the model. Our model also agrees very well with observational determinations of the SMF out to very high redshifts ($z \sim 4.5$, Fig. 9), as well as the global star formation rate history (Fig. 13). The latter clearly demonstrates how AGN feedback efficiently reduces star formation by quenching the gas cooling process at low redshifts.

(vi) Our model reproduces the abundances of observed morphological types (Conselice 2006) at all stellar masses. We notice that the morphological fractions are very sensitive to the AGN efficiency, which was set by comparing model and observed galaxy LFs, an independent statistic of the galaxy population.

(vii) Our model galaxies show a bimodal $B - V$ colour distribution up to stellar masses $M_\star \approx 10^{10.5}$–$10^{11}$ M$_\odot$. At higher masses, the distribution becomes unimodal, presenting almost only red, elliptical galaxies. This constitutes one of the main effects of AGN feedback since the original model shows a bimodal distribution for all stellar masses with an important massive, blue spiral population. The transition to a unimodal distribution is due to the passive evolution of galaxies produced after exhausting their cold gas.

(viii) We have implemented two different channels of starburst feedback: 'retention mode' and 'ejection mode' (indicating that gas is either retained or totally ejected from the galaxy halo, respectively). We found that the ejection mode provides a good agreement with all the observational constraints mentioned above. This mode does not require a recalibration of model parameters with respect to those used in sag2, in contrast to the retention mode which demands a higher AGN feedback efficiency (κ_{AGN}) in order to reproduce the observed galaxy LF; however, even after recalibrating the model, the morphological fractions in the retention mode disagree with the observational measurements. This indicates that AGN feedback during starbursts needs to be strong enough to expel the reheated gas from the galaxy halo.

(ix) We implemented the new prescriptions for merger timescales presented by J07 and B07. These prescriptions predict that major merger time-scales are significantly shorter than those arising from the estimation of LC93. As result of this, galaxies have more time to accrete gas and stars in the disc, thus producing a significantly higher number of disc instability processes than what is shown in Fig. 1. However, the net effect from applying the new time-scales is difficult to detect, and the $z = 0$ galaxy properties (e.g. galaxy LF, Fig. 15) remain almost unaffected.

Previous semi-analytic models were only focused on the analysis of particular properties of galaxies and BHs. Croton et al. (2006) present results on galaxy properties at $z = 0$, while Bower et al. (2006), Cattaneo et al. (2006) and Menci et al. (2006) also take into account properties at high redshift but without a complete analysis of BH behaviour. On the other hand, Malbon et al. (2007) make a complete analysis of BHs but do not present an analysis on galaxy properties. The combination of the different prescriptions of the BH growth and the associated AGN feedback taken from these theoretical works allowed us to develop a model that is able to reproduce several observational constraints simultaneously, focusing our analysis on different important results and predictions at low and high redshifts. We obtain similar results for the galaxy LF and colour distributions as previous models, but also obtain important differences in the evolution of the BH accretion rate; these differences may prove to be useful to obtain more clues on the

appropriate modelling and parametrization of starburst processes, chemical enrichment and AGN feedback models.

We have presented a new model of galaxy formation and evolution where we consider different mechanisms for the growth of BHs and galaxies, embedded in a ΛCDM cosmology. Among the several indicators that follow observational constraints, it has emerged that the BH and bulge growth may seem 'antihierarchical', in agreement with the downsizing scenario, even though the roots of their growth in our model is the hierarchical clustering scenario. This phenomenon deserves a detailed analysis which we will tackle in a forthcoming paper. Further modifications to the model are being developed in order to improve the treatment of the BH physics, which involves the BH spin and different physical models of accretion (e.g. Bondi 1952; Narayan, Garcia & McClintock 1997) and disc warping (e.g. Shakura & Sunyaev 1973; King et al. 2005). The implementation of these processes will give us a powerful tool to study into more detail the origin of the obscuration of QSOs and of the radio-loud QSO population, the relation between BH properties and galaxy morphology, and several other interesting observed AGN features. This will provide more links between the diverse AGN phenomenon and new underlying still unknown processes involved in the formation and evolution of galaxies.

REFERENCES

Alexander D. et al., 2003, AJ, 125, 383
Andredakis Y., Sanders R., 1994, MNRAS, 267, 283
Baldry I., Balogh M., Bower R., Glazebrook K., Nichol R., Bamford S., Budavari T., 2006, MNRAS, 373, 469
Barger A., Cowie L., Mushotzky R., Yang Y., Wang W., Steffen A., Capak P., 2005, AJ, 129, 578
Barthel P., 1989, AJ, 336, 606
Baugh C., 2006, Rep. Prog. Phys., 69, 3101
Baugh C. et al., 2004, MNRAS, 351, 44
Baugh C., Lacey C., Frenk C., Granato G., Silva L., Bressan A., Benson A., Cole S., 2005, MNRAS, 356, 1191
Bertone S., De Lucia G., Thomas P., 2007, MNRAS, 379, 1143
Binney J., Tremaine S., 1987, Nat, 326, 219B
Binney J., Gerhard O., Stark A., Bally J., Uchida K., 1991, MNRAS, 252, 210
Bondi H., 1952, MNRAS, 112, 195
Bower R., Lucey J., Ellis R., 1992, MNRAS, 254, 601
Bower R., Benson A., Malbon R., Helly J., Frenk C., Baugh C., Cole S., Lacey C., 2006, MNRAS, 370, 645
Boylan-Kolchin M., Ma C., Quataert E., 2008, MNRAS, 383, 93 (B07)
Boyle B., Terlevich R., 1998, MNRAS, 293, 49
Bruzual G., Charlot S., 2003, MNRAS, 344, 1000

Cattaneo A., 2001, MNRAS, 324, 128

Cattaneo A., Blaizot J., Devriendt J., Guiderdoni B., 2005, MNRAS, 364, 407

Cattaneo A., Dekel A., Devriendt J., Guiderdoni B., Blaizot J., 2006, MNRAS, 370, 1651

Cattaneo A., Dekel A., Faber S., Guiderdoni B., 2008, preprint (arXiv: 0801.1673)

Churazov E., Sunyaev R., Forman W., Böhringer H., 2002, MNRAS, 332, 729

Cole S., Lacey C., Baugh C., Frenk C., 2000, MNRAS, 319, 168

Cole S. et al., 2001, MNRAS, 326, 255

Conselice C., 2006, MNRAS, 373, 1389

Cora S., 2006, MNRAS, 368, 1540

Cora S., Tornatore L., Tozzi P., Dolag K., 2008, MNRAS, 386, 96

Cowie L., Songaila A., Hu E., Cohen J. G., 1996, AJ, 112, 839

Croom S., Smith R., Boyle B., Shanks T., Miller L., Outram P., Loaring N., 2004, MNRAS, 349, 1397

Croom S. et al., 2005, MNRAS, 356, 415

Croton D. et al., 2006, MNRAS, 365, 11

De Lucia G., Blaizot J., 2007, MNRAS, 375, 2

De Lucia G., Kauffmann G., White S., 2004, MNRAS, 349, 1101

De Propris R. et al. (2dFGRS Team), 2003, MNRAS, 342, 725

de Vaucouleurs G., 1991a, Sci, 254, 592

de Vaucouleurs G., 1991b, Sci, 254, 1667

Donahue M., Voit G., O'Dea C., Baum S., Sparks W., 2005, ApJ, 630, 13

Drory N., Bender R., Feulner G., Hopp U., Maraston C., Snigula J., Hill G. J., 2004, ApJ, 608, 742

Drory N., Salvato M., Gabasch A., Bender R., Hopp U., Feulner G., Pannella M., 2005, ApJ, 619, 131

Efstathiou G., Rees M., 1988, MNRAS, 230, 5

Enoki M., Nagashima M., Gouda N., 2003, PASJ, 55, 133

Erb D., Shapley A., Pettini M., Steidel C., Reddy N., Adelberger K. L., 2006, ApJ, 644, 813

Evans D. A., Hardcastle M. J., Croston J. H., 2007, in Rector T. A., De Young D., eds, ASP Conf. Ser. Vol. 386, Extragalactic Jets: Theory and Observation from Radio to Gamma Ray. Astron. Soc. Pac., San Francisco, in press (arXiv:0707.2154)

Fanaroff B., Riley J., 1974, MNRAS, 167, 31P

Feain I., Papadopoulos P., Ekers R., Middelberg E., 2007, ApJ, 662, 872

Ferrarese L., Merritt D., 2000, ApJ, 539, 9

Fine S. et al., 2006, MNRAS, 373, 613

Franceschini A., Braito V., Fadda D., 2002, MNRAS, 335, L51

Gandhi P., Fabian A. C., 2003, MNRAS, 339, 1095

Gastaldello F., Buote D., Brighenti F., Mathews W., 2007, ApJ, 673, 17

Gilli R., 2004, Adv. Space Res., 34, 2470

Giovanelli R., Haynes M., Herter T., Vogt N., da Costa L., Freudling W., Salzer J., Wegner G., 1997, AJ, 113, 53

Granato G. L., De Zotti G., Silva L., Bressan A., Danese L., 2004, ApJ, 600, 580

Gunn K., Shanks T., 1999, Adv. Space Res., 23, 1155

Häring N., Rix H., 2004, ApJ, 604, 89

Hopkins P., Hernquist L., Cox T., Di Matteo T., Robertson B., Springel V., 2006, ApJS, 163, 1

Hopkins P., Hernquist L., Cox T., Keres D., 2007, ApJS, 175, 356

Hoyle F., Fowler W., 1963, Nat, 197, 533

Huang J., Glazebrook K., Cowie L., Tinney C., 2003, ApJ, 584, 203

Jiang C., Jing Y., Faltenbacher A., Lin W., Li C., 2007, ApJ, 675, 1095 (J07)

Jolley E., Kuncic Z., 2007, Ap&SS, 310, 327

Kauffmann G., Haehnelt M., 2000, MNRAS, 311, 576

Kauffmann G., Colberg J., Diaferio A., White S., 1999a, MNRAS, 303, 188

Kauffmann G., Colberg J., Diaferio A., White S., 1999b, MNRAS, 307, 529

Kauffmann G. et al., 2003, MNRAS, 346, 1055

Kent S., 1992, ApJ, 387, 181

King A., Lubow S., Ogilvie G., Pringle J., 2005, MNRAS, 363, 49

Kochanek C. et al., 2001, ApJ, 560, 566

Lacey C., Cole S., 1993, MNRAS, 262, 627 (LC93)

Lacy M., Sajina A., Petric A., Seymour N., Canalizo G., Ridgway S., Armus L., Storrie-Lombardi L., 2007, ApJ, 669, 61

Le T., Becker P., 2007, ApJ, 661, 416

Lynden-Bell D., 1969, Nat, 223, 690

Madau P., Ghisellini G., Fabian A., 1994, MNRAS, 270, 17

Magorrian J. et al., 1998, AJ, 115, 2285

Malbon R., Baugh C., Frenk C., Lacey C., 2007, MNRAS, 382, 1394

Marconi A., Hunt L., 2003, ApJ, 589, 21

Marconi A., Risaliti G., Gilli R., Hunt L., Maiolino R., Salvati M., 2004, MNRAS, 351, 169

Marulli F., Bonomi S., Branchini E., Moscardini L., Springel V., 2008, MNRAS, 385, 1846

McGaugh S., de Blok W., 1997, ApJ, 481, 689

McLure R., Dunlop J., 2004, MNRAS, 352, 1390

Menci N., Fontana A., Giallongo E., Grazian A., Salimbeni S., 2006, ApJ, 647, 753

Mo H., Mao S., White S., 1998, MNRAS, 295, 319

Narayan R., Garcia M., McClintock J., 1997, ApJ, 478, 79

Navarro J., Frenk C., White S., 1997, ApJ, 490, 493

Nesvadba N., Lehnert M., Eisenhauer F., Gilbert A., Tecza M., Abuter R., 2006, ApJ, 650, 693

Nesvadba N., Lehnert M., De Breuck C., Gilbert A., van Breugel W., 2007, A&A, 475, 145

Norberg P. et al., 2002, MNRAS, 336, 907

Nulsen P., McNamara B., David L., Wise M., Leahy J., 2007, A&AS, 210, 3407

Percival W., Miller L., 1999, MNRAS, 309, 823

Reuland M. et al., 2007, AJ, 133, 2607

Sanders D., Mirabel I., 1996, ARA&A, 34, 749

Sanders J., 2007, Prog. Theor. Phys. Supp., 169, 16

Schawinski K., Thomas D., Sarzi M., Maraston C., Kaviraj S., Joo S., Yi S., Silk J., 2007, MNRAS, 382, 1415

Scoville N., 1999, Adv. Space Res., 23, 1033

Shakura N., Syunyaev R., 1973, A&A, 24, 337

Shankar F., Salucci P., Granato G., De Zotti G., Danese L., 2004, MNRAS, 354, 1020

Sijacki D., Springel V., di Matteo T., Hernquist L., 2007, MNRAS, 380, 877

Stern B., Poutanen J., 2008, MNRAS, 383, 1695

Soltan A., 1982, MNRAS, 200, 115

Spergel D. et al (WMAP team), 2003, ApJS, 148, 175

Springel V., 2005, MNRAS, 364, 1105

Springel V., White S., Tormen G., Kauffmann G., 2001, MNRAS, 328, 726

Springel V. et al., 2005, Nat, 435, 629

Sutherland R., Dopita M., 1993, ApJS, 88, 253

Temi P., Brighenti F., Mathews W., 2007, ApJ, 666, 222

Tremaine S., 2002, ApJ, 574, 740

Tremonti C. et al., 2004, ApJ, 613, 898

Ueda Y., Akiyama M., Ohta K., Miyaji T., 2003, ApJ, 598, 886

Wang J. M., Li Y., Wang J. C., Zhang S., 2008, ApJ, 676, 109

Wilkins S., Trentham N., Hopkins A., 2008, MNRAS, 385, 687

Wolf C., Wisotzki L., Borch A., Dye S., Kleinheinrich M., Meisenheimer K., 2003, A&A, 408, 499

This paper has been typeset from a TeX/LaTeX file prepared by the author.